# Chapter 14 Fundamentals of Aqueous Corrosion

## 14.1 Introduction

Metallic iron was first produced about 2000 years ago and has been corroding ever since. One type of *corrosion* is the reaction of a metal *M* with water that converts the surface to an oxide or hydroxide by reactions such as:

$$M + z\frac{1}{2}\,H_2O \rightarrow MO_{z/2} + \frac{1}{2}zH_2 \qquad or \qquad M + zH_2O \rightarrow M\left(OH\right)_z + \frac{1}{2}zH_2 \qquad (14.1)$$

For most metals in most environments, the oxide or hydroxide is thermodynamically more stable than the elemental metal. This is the case for iron, nickel, chromium, aluminum, zinc, uranium, and very importantly for this book, zirconium. It is not so for the noble metals, notably gold and platinum.

When a metal corrodes, the corrosion product behaves in one of several ways: i) the corrosion product may flake off the surface of the metal, exposing fresh metal for continuation of the process; this is the case for pure iron and pure zirconium; ii) the corrosion product may adhere to the metal but continue to grow with slower kinetics, as with $ZrO_2$ on Zircaloy cladding; iii) a very thin corrosion-product layer may adhere to the surface of the metal but act protectively and greatly slow the corrosion rate. This phenomenon is called *passivity* and fortunately for modern society it applies to aluminum and Fe-Ni-Cr alloys (e.g., stainless steel). [1]

Corrosion is said to be *uniform* if the product layer is of roughly the same thickness over the entire metal surface. If only special spots on the metal are susceptible to oxidation, corrosion is termed *localized*. Pits and crevices are typical of this type of corrosion. Crevices are particularly important because they may grow as cracks in response to a tensile stress parallel to the metal surface.

Additionally, the metal may corrode by dissolving as an ion in the aqueous solution by a reaction such as:

$$M + zH^+ \rightarrow M^{z+} + \frac{1}{2}zH_2 \qquad (14.2)$$

This mode of corrosion, called *active corrosion*, is particularly common in highly-acidic solutions. It is not a practical concern since the process is fast and such a combination would render useless the component in such an environment. However, the basic theory of corrosion developed in Sects 14.2 - 14.6 is based on this type of reaction.

In reactions (14.1) and (14.2), z designates the *valence* or *oxidation state* of the metal. Some metals, aluminum being one, have only a single oxidation state. Others such as iron have

[1] This phenomenon is clearly illustrated in the kitchen by the different response of carbon steel and stainless knives to water droplets. Whereas the former type of knife creates a non-adherent orange deposit (rust), the latter is not at all affected by the presence of water and remains shiny.

multiple oxidation states, all or some of which may be present as solid oxides or hydroxides coating the metal or as ions dissolved in the aqueous phase.

This chapter explores the thermodynamics, kinetics and mechanical aspects of corrosion. The thermodynamic aspects of corrosion are twofold: First, thermodynamics determines whether a particular metal is susceptible to corrosive attack by a particular aqueous solution. Second, if a metal is susceptible to corrosion, approximate thermodynamically-based constructions called *Pourbaix diagrams* show the range of conditions under which corrosion does or does not occur and which of reactions (14.1) and (14.2) is the route. These diagrams recognize the dependence of the corrosion process on the pH and the electric potential of the aqueous phase (see Section 2.9.1).

The above corrosion processes are called *overall reactions*. They do not explicitly show the transfer of electrons from one element to another. To do so requires splitting the overall reaction up into *half-cell reactions*, which clearly show the electron-transfer process. As discussed in Sect. 2.10, for reaction (14.2), these are:

$$M^{z+} + ze^{-} = M \quad and \quad 2H^{+} + 2e^{-} = H_2 \tag{14.3}$$

where $e^-$ denotes an electron. These electrons are not floating around in the solution like the ions; they are transferred directly from one species to another via the metal. Reactions of electrons and ions take place at the metal/solution interface. In reaction (14.3), each metal atom M donates z electrons to z hydrogen ions to effect the conversion to aqueous ions of $M^{z+}$ and hydrogen gas.

The $\rightarrow$ signs in reactions (14.1) and (14.2) indicate that the reaction is proceeding from left to right. The equal signs in reaction (14.3) signify that both the forward and reverse processes occur, and moreover, that they are of equal speed. That is, the reaction is in *equilibrium*. This is not always true, as half-cell reactions can proceed at finite rates. This kinetic aspect of corrosion is expressed by *Tafel diagrams*. Analysis of the kinetic mechanisms can explain the origin of these diagrams.

Localized corrosion is the attack of the metal in penetrations called *pits* or *crevices*. The former look like holes dug in the ground, and can sometimes be seen on stainless steel tableware. Crevices, on the other hand, resemble clean cracks. Crevice corrosion most frequently occurs in metals under stress, which is the origin of the name *stress-corrosion cracking (SCC)*. This phenomenon is sensitive to the pH, the electric potential and the presence of other ions in the aqueous solution. In certain alloys, chloride ions in solution significantly affect SCC. Cracks can penetrate a specimen either through the grains of the metal or follow grain boundaries. The latter is most common and is called *intergranular stress-corrosion cracking*, which is shortened to *IGSCC*. A special variant of IGSCC occurs in the coolant of nuclear reactors, in which irradiation causes sensitization of a previously immune material by irradiation induced segregation and precipitation of carbides at grain boundaries, leading to crack propagation along the Cr-depleted regions near such grain boundaries. Irradiation also creates a variety of radiolysis products that significantly accelerate the corrosion process. The term for this irradiation induced phenomenon is *irradiation-assisted stress-corrosion cracking*, or *IASCC*, and is considered in Chap. 25.

The thermodynamics and kinetics of corrosion reactions depend on temperature. Because the liquid phase is water, 25ºC is the most common temperature considered for engineering applications. One notable exception is the water coolant of a nuclear reactor( 300ºC ± 20ºC).

## 14.2 Thermodynamics of corrosion

### 14.2.1 The overall reaction

Whether corrosion of a metal is thermodynamically possible depends on the Gibbs energy change of the overall reaction. For the first of reaction (14.1), for example, this is:

$$\Delta g = g^o_{MO_{z/2}} + \tfrac{1}{2} z(g^o_{H_2} + RT \ln p_{H_2}) - g^o_M - z g^o_{H_2O} \qquad (14.4)$$

where the superscript $^o$ indicates that the substance is in its *standard state*, which is pure, at the temperature of the reaction, and at 1 atm pressure (Sect. 2.7.4). The two solids and water are pure, and so they are in their standard states. Hydrogen gas may be present at a pressure different from 1 atm, which accounts for the second term in parentheses in Eq (14.4).
Eq. (14.4) can be written as:

$$\Delta g = \Delta g^o + RT \ln p^{z/2}_{H_2} \qquad (14.5)$$

where $\Delta g^o$ is the *standard-state Gibbs energy change* of the reaction, which depends only on temperature. Reactions take place if $\Delta g$ is negative, which almost always means that $\Delta g^o$ is negative. For example, if M = Fe and z = 2, in the first of reactions (14.1), $\Delta g^o$ = -7.7 kJ/mole at 25$^o$C. Forming the equilibrium constant of the reaction as:

$$K = p_{H_2} = \exp(-\Delta g^o/RT) = \exp[-(-7700)/8.314 \times 298] = 460 \text{ atm}$$

means that the hydrogen pressure must be greater than 460 atm in order to prevent all Fe from becoming oxidized to FeO in water. On the other hand, if M = Pb, $\Delta g^o$ = 20 kJ/mole and lead contacting water could <u>not</u> be converted to PbO unless the $H_2$ pressure were less than $3 \times 10^{-8}$ atm. The standard-state Gibbs energy simply indicates whether the left-hand side or the right-hand side of the written reaction, (of which (14.1) and (14.2) are examples), is favored.

### 14.2.2 Pourbaix diagrams

More detailed information about the thermodynamics of a particular metal in water is contained in *Pourbaix diagrams*, named after the Russian chemist who produced a PhD thesis on the graphical representation of the role of the pH and electric potential of an aqueous solution on the stable states of the contained metal. Pourbaix diagrams are also known as *pH-potential diagrams*. They are essentially plots of the Nernst equation (Eq (2.88)). For the half cells of Eq (14.3) at 25$^o$C, these are:

$$\varphi^N_M = \varphi^o_M - \frac{0.059}{z} \log\left(\frac{1}{[M^{z+}]}\right) \quad \textit{and} \qquad \varphi^N_H = \varphi^o_H - \frac{0.059}{2} \log\left(\frac{p_{H2}}{[H^+]^2}\right) \qquad (14.6)$$

where $\phi^{o}_{M}$ is the standard electrode potential (Table 2.2) and $[M^{z+}]$ is the molar concentration of the metal ion. z is the number of electrons transferred in the $M/M^{z+}$ half-cell reaction . Similar assignments are made for the hydrogen half-cell, for which the number of transferred electrons is 2.

The rules for using Nernst equations to construct Pourbaix diagrams are:

i) the pressures of the gases $H_2$ and $O_2$ are set equal to 1 atm
ii) the concentrations of all ions (excepting $H^+$) are fixed at $10^{-6}$ M.
iii) pure solids and liquid water do not appear in Eq (14.6) because their activities are unity.
iv) The standard electrode potentials $\phi^o$ are obtained from Table 2.2.

The choice of $10^{-6}$ M is an arbitrary demarcation of the onset of corrosion. The anions that accompany the various cations (e.g., $Cl^-$, $SO_4^{2-}$) are ignored.

In Pourbaix diagrams the metal can exist in two states: dissolved (as ions) or solid, including metal, metal oxide(s), hydroxides and oxy-hydroxides. For iron, the important species are the ions $Fe^{2+}$, $Fe^{3+}$, $Fe(OH)^+$, $Fe(OH)_3^-$ and $FeO_4^{2-}$ and the solids Fe, $Fe_3O_4$ and $Fe_2O_3$.

$Fe_3O_4$ (magnetite) has a *spinel* crystal structure (see Sect. 3.8.5). Magnetite ($Fe^{2+}Fe_2^{3+}O_4$) is a special case of the many two-metal oxides with this structure and the general formula $(Fe_x^{2+}M_{1-x}^{2+})(Fe_{2-y}^{3+}Cr_y^{3+})O_4$ where M is a divalent cation (Fe, Ni, Co, Zn).

An example of constructing the Pourbaix for iron is shown in Table 14.1 and Fig. 14.1. The two horizontal lines (nos. 1 and 2) and the vertical line (no. 4) and the sloped line (no.3) are shown on the $Fe/H_2O$ Pourbaix diagram of Fig. 14.1 along with the remainder of the iron-water lines. The lines represent the equilibria or the phase boundary between different chemical species formed in the reaction specified.

**Table 14.1 Construction of the iron/water Pourbaix diagram at 25°C (Eq. (14.6))**

| Line No. | couple | Half-cell reaction | Standard potential, $\phi^{o}$ @ | Pourbaix (Nernst) line |
|---|---|---|---|---|
| 1 | $Fe/Fe^{2+}$ | $Fe^{2+} + 2e = Fe$ | -0.44 | $\phi = - 0.62$ |
| 2 | $Fe^{2+}/Fe^{3+}$ | $Fe^{3+} + e = Fe^{2+}$ | 0.77 | $\phi = 0.77$ |
| 3 | $Fe^{2+}/Fe_2O_3$ | $Fe_2O_3 + 6H^+ + 2e = 2Fe^{2+} + 3H_2O$ | 0.68* | $\phi = 1.03 - 0.18pH$ |
| 4 | $Fe^{3+}/Fe_2O_3$ | $2Fe^{3+} + 3H_2O = Fe_2O_3 + 6H^+$ | # | $pH = 1.5^{\#}$ |
| 5 | $Fe^{2+}/Fe_3O_4$ | $Fe_3O_4 + 8H^+ + 2e = 3Fe^{2+} + 4H_2O$ | 1.0 | $\phi = 1.53 – 0.24pH$ |
| 6 | $Fe/ Fe_3O_4$ | $Fe_3O_4 + 8H^+ + 8e = 3Fe + 4H_2O$ | - 0.08 | $\phi = -0.08 – 0.06pH$ |
| 7 | $Fe_2O_3/ Fe_3O_4$ | $3Fe_2O_3 + 2H^+ + 2e = 2Fe_3O_4 + H_2O$ | 0.22 | $\phi = 0.22 – 0.06pH$ |
| a | $H^+/H_2$ | $2H^+ + 2e = H_2$ | 0 | $\phi = - 0.06pH$ |
| b | $O_2/H_2O$ | $1/2O_2 + 2H^+ + 2e = H_2O$ | 1.23 | $\phi = 1.23 - 0.06pH$ |

@ From Table 2.2 except for Nos. 3 – 7
* see example in Sect. 2.10.3
# see Example #2 below

The $H^+/H_2$ line in the Pourbaix diagram (Line a) is especially important in the cooling water of the reactor. In a PWR the $H_2$ pressure in the primary circuit can be adjusted at will. In a BWR, however, the $H_2$ is mixed with steam so the $H_2$ pressure is less than the total pressure and the electrical potential is lower than that established in a PWR.

Example #1 Line 3 in Table 14.1
The Nernst equation for No. 3 is:

$$\phi_3^N = \phi_3^o - \frac{0.059}{2}\log\left(\frac{[Fe^{2+}]^2}{[H^+]^6}\right) = 0.68 - \frac{0.059}{2}\left(-6\log[H^+] + 2\log[10^{-6}]\right) = 0.68 - 0.18pH + 0.35$$

Example #2 Line 4 in Table 14.1
line No. 4 does not involve electrons, so it does not have a standard electrode potential. It must be treated like reaction (a) in example7b in Sect. 2.10.2:
In Table 2.2, half-cell reactions 2×(9) - (15) give reaction No. 4 in Table 14.1. Using Eq (2.82):

$$\Delta\mu_4^o = 2\Delta\mu_9^o - \Delta\mu_{15}^o - = 2(-1)(96.5)\phi_9^o - (-2)(96.5)\phi_{15}^o = (-2)(96.5)(0.77) - (-2)(96.5)(0.68) - = -17.4\ \frac{kJ}{mole}$$

By analogy to Eq (2.73b):

$$\Delta\mu_4^o = -RT\ln\left([H^+]^6/[Fe^{3+}]^2\right) = -8.314\times 0.298\ln\left([H^+]^6/[Fe^{3+}]^2\right) = -5.75\log\left([H^+]^6/[Fe^{3+}]^2\right)$$
$$= -5.75\left(6\log[H^+] - 2\log[Fe^{3+}]\right) = -5.75\left(-6\,pH - 2\log(10^{-6})\right) = -5.75(-6\,pH + 12)$$

Equating the right-hand sides of the above equations: -5.75(-6pH + 12) = -17.4. Solving: **pH = 1.5.**
This is line 4 in Fig. 14.1.

The lines a and b in Fig. 14.1 encompass the zone of stability of water. For potentials less than line **a**, water decomposes into $H_2$ and $OH^-$ by half-cell reaction 3 in Table 2.2. The standard electrode potential of this half-cell reaction is $\phi_a^o = 0$

$$j_a^N = j_a^o - \frac{0.059}{2}\log\left(\frac{p_{H2}}{[H^+]^2}\right) = 0 + 0.059\log[H^+] = -0.059\,pH$$

The dashed line **a** in Fig. 14.1 and the second equality the above equation correspond to an $H_2$ pressure of 1 atm. For $p_{H2}$ in the above equation greater than 1 atm lowers line **a** until metallic Fe is stable in liquid water.

For potentials greater than line b in Fig. 14.1, water decomposes into $O_2$ and $H^+$ by half-cell reaction b in Table 14.1, for which the standard electrode potential is $\phi_b^o$ = 1.23 V. This leads to the Nernst equation shown in the last row of the last column in Table 14.1.

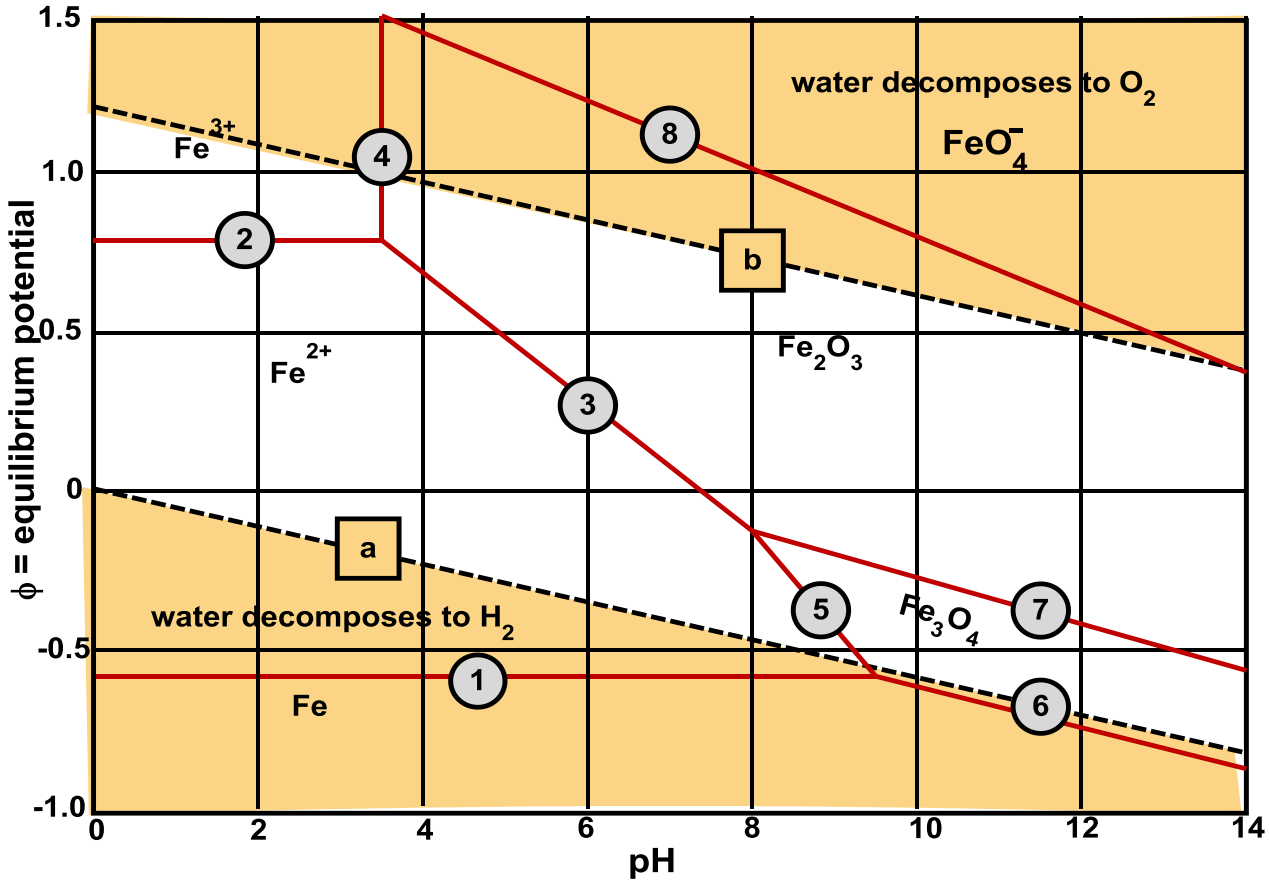


**Fig. 14.1 Pourbaix diagram for iron/water at 25°C**

Limitations of Pourbaix diagrams for assessing corrosion of metals in water include:

1. Usually, but not always, pure metals are treated – e,g,, iron in Fig. 14.1

2. It is based on thermodynamics only, containing no information on the kinetics of corrosion
3. Concentrations of all ionic species are $10^{-6}$ M; all gases are 1 atm. However, Pourbaix diagrams can be constructed for different values of these parameters.
4. Conditions placing a system in an oxide does not mean that the oxide is stable mechanically; it may not form a protective scale.
5. The diagram is based on information for a specific temperature and total pressure
6. Nonideality is neglected; activities are approximated by concentrations

## 14.3 The electrode potential at equilibrium

The full cell in Fig. 14.2(a) is similar to that in Fig. 2.10 with the right-hand half-cell a *standard hydrogen electrode* (acronym SHE, Sect. 2.10.1). The SHE is connected to the $M/M^{z+}$ half-cell by a voltmeter, and so measures the equilibrium electrode potential, the Nernst potential $\phi_M^N$ with $\phi_{SHE} = 0$ (Section 2.10.3):

$$\phi_M^N = \phi_M^o - \frac{RT}{zF}\ln\left(\frac{1}{[M^{z+}]}\right) = \phi_M^o + \frac{0.059}{z}\log[M^{z+}] \qquad (2.85a)$$

The second form of Eq (2.85a) uses appropriate values of the gas constant R and Faraday's constant F at T = 298 K. The natural logarithm has been converted to base-10.

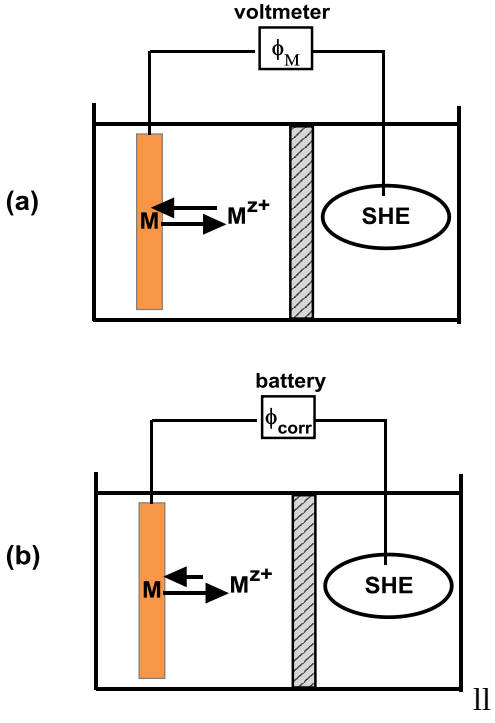


**Fig. 14.2 Electrochemical cell to measure the electric potential of the $M/M^{z+}$ | SHE cell**

Another way of representing equilibrium in the metal half cell is by equating the rates of the *anodic* reaction $M \rightarrow M^{z+} + ze^-$ and the *cathodic* reaction $M^{z+} + ze^- \rightarrow M$. "Anodic" denotes oxidation, or increase in valence, while "cathodic" is synonymous with reduction (decrease in valence).

The solid curve in Fig. 14.3 represents the Gibbs energy of the metal atom as it becomes ionized and moves under the equilibrium conditions of Fig. 14.2(a) to and from the M electrode and the solution. By the definition of equilibrium, the Gibbs energies of M and $M^{z+}$ are equal.

The anodic and cathodic M-atom/ion fluxes are:

$$j_a^{eq} = k_a^o \exp\left(-\frac{\Delta g^*}{RT}\right) \tag{14.7}$$

and

$$j_c^{eq} = k_c^o \exp\left(-\frac{\Delta g^*}{RT}\right)[M^{z+}] \tag{14.8}$$

where $k_a^o$ and $k_c^o$ are the pre-exponential factors for the anodic and cathodic rate equations. j is the flux (moles per unit time per unit area) to or from the metal surface and the bulk solution. The subscript **a** means anodic ($M \rightarrow M^{z+}$) and the cathodic reaction ($M^{z+} \rightarrow M$) is indicated by the subscript **c**. The superscript *eq* signifies equilibrium.

As indicated by the equal-length arrows in Fig. 14.2(a), at equilibrium,

$$j_a^{eq} = j_c^{eq} = j_{eq} \tag{14.9}$$

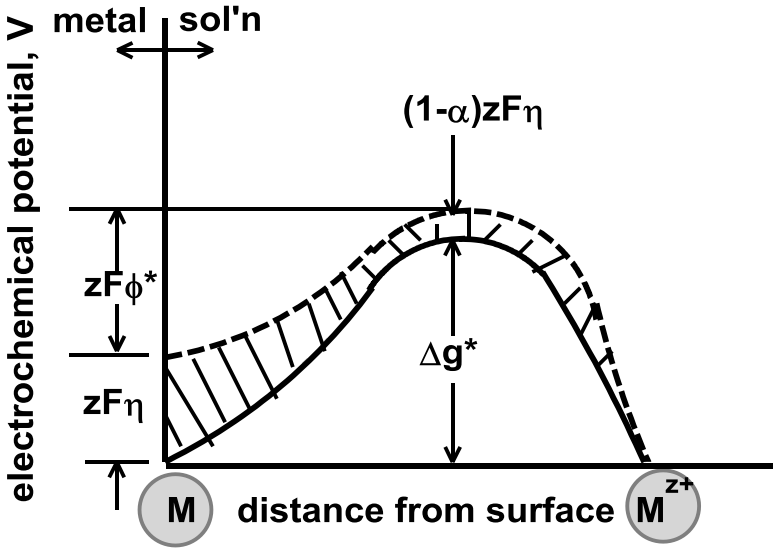


**Fig. 14.3 Gibbs energy barrier for $M \rightarrow M^{z+} + ze^-$ and $M^{z+} + ze^- \rightarrow M$**

**Solid curve: at equilibrium; dashed curve: with potential**
**(F is Faraday's constant)**

## 14.4 Corrosion kinetics

### 14.4.1 The Butler-Volmer equation

The *electric potential* plays a central role in corrosion kinetics. It is analogous to the chemical potential, the thermal potential and the mechanical potential; all of these have in common that a gradient of the potential causes motion of some quantity: the chemical potential drives material species; the thermal potential drives heat[2]; the mechanical potential drives massive objects. The electric potential drives charged species, either electrons in a wire or ions in an aqueous solution.

In Fig. 14.2(b), the voltmeter in Fig. 14.2(a) is replaced by a voltage source (a battery) that applies an arbitrary potential, which will be called $\phi_{corr}$. Assuming that $\phi_{corr} > \phi_M^N$, dissolution of the metal electrode, or *corrosion*, begins. As indicated by the size of the two arrows in the metal half cell of Fig. 14.2(b), the rate of the anodic reaction $M \rightarrow M^{z+} + ze^-$ now exceeds the rate of the cathodic reaction $M^{z+} + ze^- \rightarrow M$. If the metal remains bare (i.e., no oxide film), the process is called *active corrosion.* This is the process that will be discussed first.

The difference between the rates of the anodic ($j_a$) and cathodic ($j_c$) reactions is the corrosion rate:

$$j = j_a - j_c \tag{14.10}$$

However, if the cathodic reaction is a or b in Table 14.1, $j_c$ does not appear in Eq (14.10) because these lines do not involve reduction of metal ions to metal.

To understand corrosion kinetics, we examine the Gibbs energy of the metal/ion as it moves along the dashed curve in Fig. 14.3. This curve shows the effect on the rates of the forward and reverse steps on the deviation of the potential, $\phi$, from the Nernst potential, called the *overpotential*,

$$\eta = \phi - \phi_M^N \tag{14.11}$$

The overpotential can be positive or negative. The dashed curve in Fig. 14.3 starts out at the metal surface with a potential (now electrochemical) at a Gibbs energy $z\mathbf{F}\eta$ higher than the equilibrium value for M. This added potential decreases with distance into the solution so that after a few nanometers, none of it remains. The dashed and solid curves at the maximum differ from the value at the metal-solution interface by a fraction 1-$\alpha$, where $\alpha$ is approximately ½. The activation energy for the forward step with the interface potential is obtained from the plot as:

$$z\mathbf{F}\eta_a + z\mathbf{F}\phi^* = \Delta g^* + (1-\alpha)\, z\mathbf{F}\eta \quad \text{or} \quad z\mathbf{F}\phi^* = \Delta g^* - \alpha z\mathbf{F}\eta$$

With this change, the anodic rate becomes:

$$j_a = k_a^o \exp(-zF\varphi^*/RT) = \vec{k}_a^o \exp(-\Delta g^*/RT)\exp\{\alpha\, zF\eta/RT\} \tag{14.12}$$

[2] Note that these are the diagonal terms in the Onsager relations; it is also possible for example for a themal gradient to drive material transport, as in the *Soret effect.*

Including the interface potential, the new activation energy in the opposite direction is $\Delta g^o + \Delta g^* + (1-\alpha)z\mathbf{F}\eta$, or the reverse rate is:

$$j_c = k_c^o[M^{z+}]\exp[-\Delta g^*/RT]exp\{-(1-a)z\mathbf{F}\eta RT\} \tag{14.13}$$

The corrosion rate is given by Eq (14.10). Dividing Eq (14.12) by Eq (14.7) and Eq (14.13) by the Eq (14.8) yields the *Butler-Volmer equation*:

$$\frac{j}{j_{eq}} = \frac{i}{i_o} = \exp\left[\frac{\alpha zF\eta}{RT}\right] - \exp\left[-\frac{(1-\alpha)zF\eta}{RT}\right] \tag{14.14}$$

where *i* is the *current density*:

$$i\ \left(A/cm^2\right) = z\mathbf{F}j \tag{14.15}$$

for $i_o$, see Sect. 14.4.3.

Given a positive overpotential η, the corrosion rate j or the corrosion current i can be calculated from Eq (14.14) if $i_o$ and α are known. Similarly, if $\eta < 0$, the current i becomes a measure of the metal deposition rate.

Figure 14.4 shows data for the half-cell $Fe = Fe^{2+} + 2e^-$ in acid of pH =2 at $25^OC$. The points have been fitted to Eq (14.14) with one modification: the current i is changed to positive when the potential η is negative.

An equation analogous to (14.14) applies to all half-cell reactions involving the metal and solution species or on the metal between solution species. An example of the latter is the $H^+/H_2$ half-cell reaction of Eq (14.3), which, although involving only solution species, occurs on the surface of the metal in the solution.

### 14.4.2 Tafel equations

At large absolute values of the overpotential, either the first or the second term in Eq (14.14) predominates. The anodic line ($\eta > 0$) contains the first term only; the second term quickly becomes negligible as the potential becomes positive and Eq (14.14)reduces to the anodic line:

$$\eta = \beta_a \log\left(\frac{i_a}{i_o}\right) \qquad where \qquad \beta_a = \frac{2.3RT}{\alpha\, z\, F} \tag{14.16}$$

When the potential η is negative, the second term on the right-hand side of Eq (14.14) predominates, and the cathodic straight line in Fig. 14.4 is:

$$\eta = -\beta_c \log\left(\frac{i_c}{i_o}\right) \qquad where \qquad \beta_c = \frac{2.3RT}{(1-\alpha)\, z\, F} \tag{14.17}$$

The simplified forms of the Butler-Volmer equation given by Eqs (14.16) and (14.17) are called the *Tafel equations.* They form the basis of analyzing corrosion kinetics.

A half-cell reaction can be either anodic or cathodic, depending on the concentrations of solution species and the other active half-cell reactions. There must be at least two half-cell reactions in a real system.

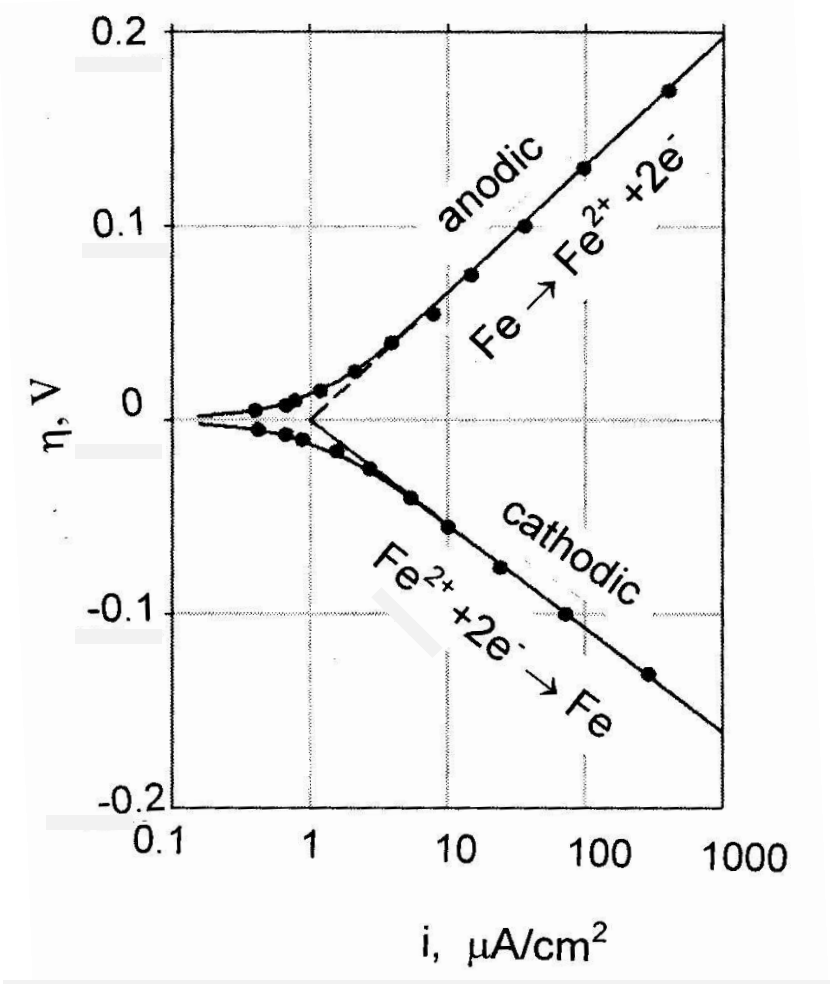


**Fig. 14.4 Current density for the Fe/Fe$^{2+}$ half cell and fit to the Butler-Volmer equation**

### 14.4.3 The exchange current density $i_o$

In Eq (14.14) $i_o$ is the *exchange current density*, which corresponds to the flux $j_{eq} = i_o / z\mathbf{F}$. $i_o$ is a kinetic parameter that is strongly dependent on the metal. For the reaction $2H^+ + 2e^- \leftrightarrow H_2$, it is:

| electrode | $i_{oH}$, A/cm$^2$ |
|---|---|
| Pt | $10^{-3}$ |
| Fe | $10^{-6}$ |
| Hg | $10^{-12}$ |

The exchange-current-density concept is applicable to any combination of half-cell reaction and electrode. For the half-cell reaction, $M^{z+} + ze^- \leftrightarrow M$, $i_{oM}$ also depends on the metal, and is

different from $i_{oH}$. For the $Fe/Fe^{2+}$ half-cell (Fig. 14.4), $i_{oFe}$ is the intersection of the extrapolations of the anodic and cathodic lines at 1 $\mu A/cm^2$. This is (fortuitously) the same current density contained in the above table for the $H_2/H^+$ half cell.

### 14.4.4 The symmetry parameter

The parameter $\alpha$ in the Butler-Volmer equation is contained in the slopes of the Tafel lines.

Example #3 Determination of the best-fitting value of $\alpha$ for the $Fe/Fe^{2+}$ half cell using Fig. 14.4
For this half-cell, z = 2. At 25°C, 2.3RT/F = 2.3(8.314)(298)/96,500 = 0.059.
From Eq (14.13a) the slope of the anodic line is:

$$\beta_a = \frac{2.3\,RT/F}{2\times\alpha_{Fe}} \text{ or } \frac{0.059}{2\times\alpha_{Fe}} = \frac{0.193}{\log(1000)} = 0.065, \quad \text{which gives } \alpha_{Fe} = 0.45$$

The slope of the cathodic branch is:

$$\beta_c = \frac{2.3\,RT/F}{2\times(1-\alpha_{Fe})} \quad \text{or} \quad \frac{0.059}{2\times(1-\alpha_{Fe})} = \frac{0.16}{\log(1000)} = 0.053, \quad \text{or } \alpha_{Fe} = 0.45$$

Agreement of the values of $\alpha_{Fe}$ from the anodic and cathodic polarization curves is excellent.

### 14.4.5 Analyzing corrosion reactions quantitatively

The previous section dealt with individual half-cell reactions, which were caused to proceed in either the anodic or cathodic direction by application of the appropriate overpotential (positive or negative) to the electrochemical cell. However, in actual corrosion situations, a metal (e.g., a pipe or tubing through which water flows) supports the anodic reaction $M \rightarrow M^{z+} + z\,e^-$ along with a cathodic reaction, which can be the reverse of any one of the half-cell reactions 1 – 3a in Table 2.2.

Figure 14.5 is a schematic of water flowing through a pipe. The water is sufficiently acidic that the metal of the pipe wall undergoes active corrosion (i.e. without formation of an oxide scale on the surface). Electrons produced by the anodic reaction flow through the pipe wall to the zone where the cathodic reaction, in this case reduction of protons, is occurring. The pipe is connected to a standard hydrogen electrode (SHE) for the purpose of measuring the potential (i.e., the pipe is corroding). The SHE is connected to the pipe water by a salt bridge, the function of which is to complete the electrical circuit of the measuring cell.

Determination of the corrosion rate requires coupling of the anodic (corrosion) half-cell reaction with the appropriate cathodic half-cell reaction. $2H^+ + 2e^- \rightarrow H_2$ will be employed for purposes of illustrating how both half-cell reactions operate together spontaneously. (Reaction b in Table 14.1 could also be an important cathodic half-cell reaction).

The analytic method is applied to corrosion of zinc in acid at 25°C, which proceeds according to:

$$Zn + 2H^+ \rightarrow Zn^{2+} + H_2$$

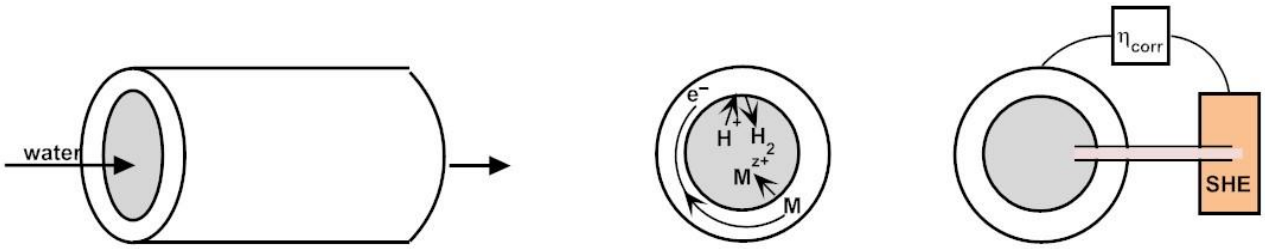


**Fig. 14.5 Corrosion of a pipe in flowing water.**

This overall reaction consists of the half-cell reactions:

anodic: $Zn \rightarrow Zn^{2+} + 2e$ and cathodic: $2H^{+} + 2e \rightarrow H_2$

The current-potential relation for the zinc half-cell reaction is taken from Eq (14.16)

$$log\left(i_{aZn}\right) - log\left(i_{oZn}\right) = (\phi - \phi_{Zn}^{N}) / \beta_{aZn} \tag{14.18}$$

where $i_{oZn}$ is the exchange current density for $Zn/Zn^{2+}$ and:

$$\beta_{aZn} = \frac{2.3RT}{2\alpha_{Zn}F} = \frac{0.059}{2\alpha_{Zn}} \tag{14.19}$$

$\phi_{Zn}^{N}$ is the Nernst potential:

$$\phi_{Zn}^{N} = \phi_{Zn}^{o} + \frac{RT}{2F}\ln[Zn^{2+}] = \phi_{Zn}^{o} + \frac{0.059}{2}\log[Zn^{2+}] \tag{14.20}$$

For the cathodic branch of the $H_2/H^{+}$ half-cell, Eq (14.17) converts to:

$$log\left(i_{cH}\right) - log\left(i_{oH}\right) = -(\phi - \phi_{H}^{N}) / \beta_{cH} \tag{14.21}$$

where $i_{oH}$ is the exchange current density for $H_2/H^{+}$ and:

$$\beta_{cH} = \frac{2.3RT}{(1-\alpha_H)F} = \frac{0.059}{1-\alpha_H} \tag{14.22}$$

$\phi_{H}^{N}$ is the Nernst potential:

$$\phi_{H}^{N} = 0.059\log\left(\frac{[H^{+}]}{p_{H2}^{1/2}}\right) \tag{14.23}$$

Assuming that the two half-cell reactions occur on the same (or equal) surface areas, conservation of charge requires that $i_{aZn} = i_{cH} = i_{corr}$ at $\phi = \phi_{corr}$, the corrosion potential. Applying this equality to Eqs (14.18) and (14.21) and solving for $\phi_{corr}$ yields:

$$\phi_{corr} = \frac{\log(i_{oH}) - \log(i_{oZn}) + \phi_{H}^{N}/\beta_{cH} + \phi_{Zn}^{N}/\beta_{aZn}}{1/\beta_{cH} + 1/\beta_{aZn}} \tag{14.24}$$

from which the corrosion current can be obtained from Eqs (14.18) or (14.21)

Example #4 Analytical method applied to corrosion of zinc in acid
The solution composition is pH = 0 ($[H^+]$ = 1 M), $p_{H2}$ = 1 atm and $[Zn^{2+}]$ = 1 M. The exchange current densities are $i_{oH} = 10^{-10}$ A/cm$^2$ and $i_{oZn} = 8\times10^{-8}$ A/cm$^2$. The symmetry factors are $\alpha_{Zn}$ = 0.36 and $\alpha_H$ = 0.23. The standard electrode potential for Zr (from Table 2.2) is $\phi^o_{Zn} = -0.76$ V. Equations (14.19) and (14.22) give $\beta_{aZn}$ = 0.082 and $\beta_{cH}$ = 0.076. With the solution composition and Eqs (14.20) and (14.23) $\phi^N_{Zn}$ = -0.76 V and $\phi^N_H$ = 0 V. Substituting in Eq (14.16) yields $\phi_{corr}$ = -0.48 V and either Eq (14.18) or (14.21) gives $i_{corr} = 2\times10^{-4}$ A/cm$^2$

### 14.4.6 Evans plots
Graphical solutions of the Tafel equations are called *Evans plots*. They involve on one graph a plot like Fig. 14.4 for the metal and the equivalent plot for the oxidizing component ($H^+$ or $O_2$).

Because the Nernst potentials are different for the two ions, the ordinate of the Evans plot cannot be the potential $\eta$ as in Fig. 14.4. In order to accommodate the two different half-cell reactions, all potentials are expressed relative to the SHE.

Figure 14.6 shows the Evans plot for zinc dissolution in acid using the properties and parameters of Example #4. The intersection of the anodic zinc line and the cathodic hydrogen line gives the same results as obtained from Eq (14.16). The slight curvature near the exchange current density seen in Fig. 14.4 is ignored.

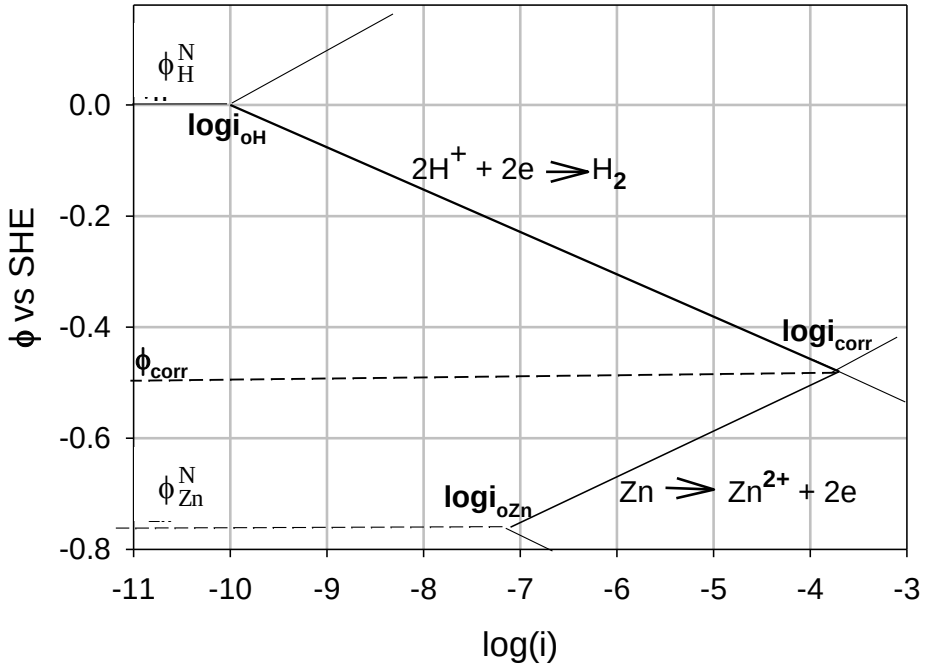


**Fig. 14.6 Evans plot for Zn corrosion in acid**

### 14.4.7 Evans plots for multiple cathodic reactions
In many situations, active corrosion is driven by more than a single cathodic or anodic reaction.

As an example we examine the electrochemistry of water filling a glass container. The water is saturated with $O_2$ at 0.5 atm and $H_2$ at 0.1 atm and contains $H_2O_2$ at a concentration of $10^{-3}$ M. The pertinent half-cell reactions, their standard electrode potentials and exchange current densities are:

| | Half-cell Reaction | $\phi^o$, V | $i_o$, A/cm$^2$ | $\alpha$ | Expected Type |
|---|---|---|---|---|---|
| 1. | $½O_2 + 2H^+ + 2e = H_2O$ | 1.23 | 2e-6 | 0.5 | Cathodic |
| 2. | $H_2O_2 + 2H^+ + 2e = 2H_2O$ | 1.77 | 4e-8 | 0.5 | Cathodic |
| 3. | $2H^+ + 2e = H_2$ | 0 | 4e-8 | 0.5 | Anodic |

In the last column of the above table, the half-cell reactions are assigned a direction. This assignment is based on the assumption that the standard electrode potentials of the first two reactions are large enough that their Nernst potentials will be greater than the corrosion potential. In this case, the overpotentials are negative, which means that the cathodic Tafel reactions (Eq (14.13b)) apply. Of course this assumption must be checked in the analysis.

If there are no reactions with the container surface, what is the *electrochemical potential* (ECP) of the water?

The Nernst equations for these half-cell reactions at 25$^o$C (Eq (2.88)) are:

$$\begin{aligned}
\phi_1^N &= \phi_1^o - \frac{0.059}{2}\log\left(\frac{1}{[p_{O2}]^{1/2}[H^+]^2.}\right) = 1.23 + 0.059\log\left([p_{O2}]^{1/4}[H^+]\right) \\
\phi_2^N &= \phi_2^o - \frac{0.059}{2}\log\left(\frac{1}{[H_2O_2][H^+]^2.}\right) = 1.77 + 0.059\log\left([H_2O_2]^{1/2}[H^+]\right) \\
\phi_3^N &= \phi_3^o - \frac{0.059}{2}\log\left(\frac{p_{H2}}{[H^+]^2}\right) = 0 + 0.059\log\left(\frac{[H^+]}{p_{H2}^{1/2}}\right)
\end{aligned} \qquad (14.25)$$

For the specified component concentrations,

$$\phi_1^{\mathrm{N}} = 1.23 + 0.059\log\left([0.5]^{1/4}10^{-7}\right) = 0.81\ \mathrm{V}$$

$$\phi_2^{\mathrm{N}} = 1.77 + 0.059\log\left([10^{-3}]^{1/2}[10^{-7}]\right) = 1.27\ \mathrm{V}$$

$$\phi_3^{\mathrm{N}} = 0 + 0.059\log\left(\frac{[10^{-7}]}{\sqrt{0.1}}\right) = -0.38\ \mathrm{V}$$

The Butler-Volmer equations (Eq (14.14)) for the individual current densities of the half-cell reactions are:

$$i_j = i_{oj}\left[\exp\left(\frac{\phi-\phi_j^N}{\beta}\right) - \exp\left(-\frac{\phi-\phi_j^N}{\beta}\right)\right] \qquad j = 1,2,3 \qquad (14.26)$$

where

$$\beta = \frac{RT/F}{\alpha z} = \frac{8.314 \times 298/96.5 \times 10^3}{0.5} = 0.052\,V \qquad (14.27)$$

z = 1 because the moving ion in all three half-cell reactions in the above table is $H^+$.

The ECP ($\phi$ in Eq (14.26)) is determined by substituting the Nernst potentials and exchange current densities in Eqs (14.26) and solving the charge balance:

$$i_1 + i_2 + i_3 = 0 \qquad (14.28)$$

In view of the Nernst potentials calculated above, the ECP lies between $\phi_1^N$ and $\phi_3^N$. Therefore, the exponential terms in Eq (14.26) can be simplified as follows:
For j = 1 and 2, $\phi - \phi_j^N{}_j$ is negative, so the first exponential terms can be neglected, and the current densities are of the cathodic Tafel type, Eq. (14.17):

$$i_1 = -2\times10^{-6}\exp[-(\phi - 0.81)/0.052] \qquad i_2 = -4\times10^{-8}\exp[-(\phi - 1.27)/0.052]$$

Since $\phi - \phi_3^N$ is positive, the second exponential term in Eq (14.26) is negligible and the anodic Tafel equation is:

$$i_3 = 4\times10^{-8}\exp[(\phi + 0.38)/0.052]$$

Substituting the above equations for $i_j$ into Eq (14.28) and solving (by trial-and-error) gives $\phi = \phi_{corr} = 0.443$ V.

The information in the above table permits construction of an Evans plot for the three half-cell reactions. If β is the same for all half-cell equations, the slopes of the lines are all equal in magnitude. Figure 14.7 shows the Evans diagram for this system. The labels 1, 2 and 3 refer to the half-cell reactions in the table at the beginning of this section.

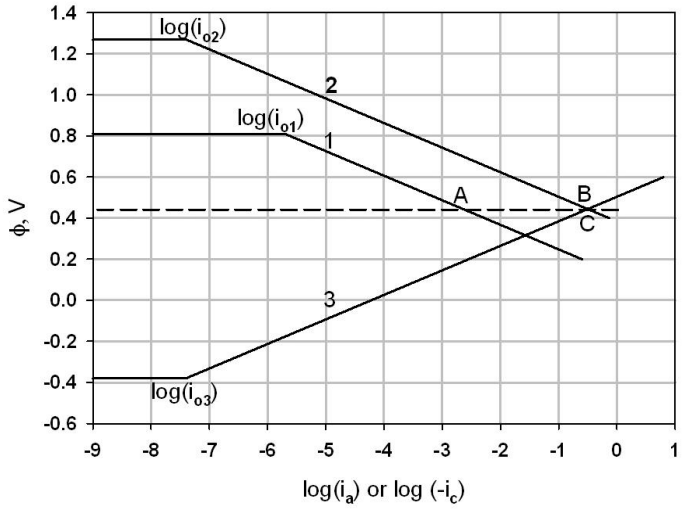


**Fig. 14.7 Evans diagram with two cathodic half-cells**

The dashed line is moved up and down until Eq (14.28) is satisfied. Because half-cell reaction No. 1 contributes negligibly to the current balance (the intersection of lines 1 and 3 occurs at a current density an order of magnitude smaller than point B/C), the result is dominated by half-cell reactions 2 and 3, which intersect at point B/C. The following table compares the results of the analytic and graphical solutions. The results from the two methods are in excellent agreement. The graphical method is essentially equivalent to the analytic method, but it is less accurate because it requires reading values from the Evans diagram.

| | | $A/cm^2$ | | |
|---|---|---|---|---|
| **Method** | **$\phi$, V** | **$-i_1$** | **$-i_2$** | **$i_3$** |
| Analytic | 0.443 | 0.003 | 0.31 | 0.32 |
| Graphical | 0.44 | 0.0025 | 0.32 | 0.315 |

### 14.4.8 Evans plots for multiple anodic reactions

A common case of two anodic reactions and one cathodic reaction is zinc plated on iron, which constitutes *galvanic protection*. Figure 14.8 is an Evans plot wherein these two metals exist in the presence of oxygenated neutral water, which provides the cathodic half-cell:

$$\frac{1}{2}O_2 + 2H^+ + 2e^- \rightarrow H_2O. \qquad (14.29)$$

The areas of the two metals exposed to water may be different, so the electron-production/electron consumption balance is:

$$(A_{Fe} + A_{Zn})\, i_{O2} = A_{Fe} i_{Fe} + A_{Zn} i_{Zn}$$

where $A_{Fe}$ and $A_{Zn}$ are the areas of the two metals exposed to water. The above charge balance assumes that the cathodic reaction takes place over the entire exposed metal area. With reference to Fig. 14.8, the relevant terms in the above equation are:

$$i_{O2} = 10^C \qquad i_{Fe} = 10^A \qquad i_{Zn} = 10^B$$

which is a significantly smaller iron loss rate ($10^A$) than would afflict unprotected iron ($10^D$).

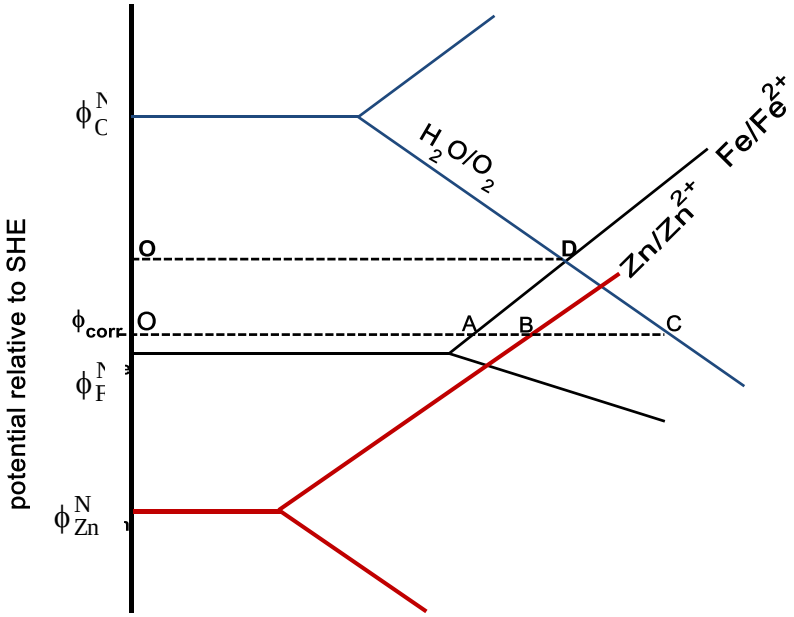


**Fig. 14.8 Galvanic corrosion - Zinc-coated iron in oxygenated neutral water**

### 14.4.9 Concentration polarization

The cathodic polarization curves heretofore represented as straight lines with a negative slope are surface reactions whose rates depend upon delivery of a dissolved species from the bulk solution to the interface. Like any other reaction at a surface supplied with reactants from a fluid, they are potentially mass-transfer limited. Consider the cathodic half-cell reaction $2H^+ + 2e^- \rightarrow H_2$. The transport rate of $H^+$ to the surface depends on the hydrodynamic boundary layer in the water adjacent to the metal and on the diffusivity of $H^+$ in water. Figure 14.9 is a sketch of the $H^+$ concentration close to the surface.

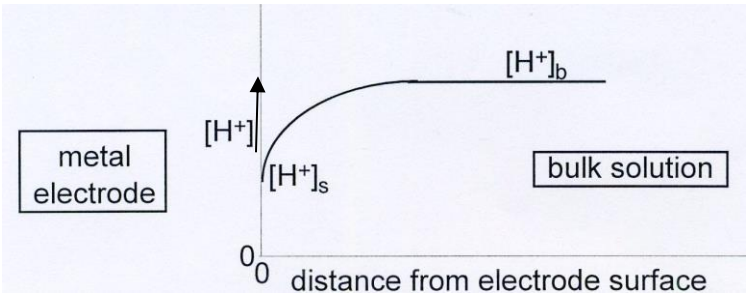


**Fig. 14.9 Concentration of $H^+$ adjacent to the metal surface during active polarization**

The flux of $H^+$ to the interface ($j_{MT}$), or the equivalent current density ($i_{MT}$), is :

$$j_{MT} = k_{MT}\left(\left[H^+\right]_b - \left[H^+\right]_s\right) = i_{MT} / \mathbf{F} \qquad (14.30)$$

where $k_{MT}$ is the *mass transfer coefficient* between the bulk coolant and the metal surface.

$[H^+]_b$ is the bulk concentration of hydrogen ions and $[H^+]_s$ is the concentration at the surface.

$i_{MT}$ must be the same as the cathodic current $i_{cH}$ in the Tafel equation, Eq (14.17)

$$\phi - \phi_{HS}^N = -\beta_{cH} \log\left(\frac{i_{cH}}{i_{oH}}\right)$$
$$\text{where, at } 25^o C, \qquad \beta_{cH} = \frac{2.3RT}{(1-\alpha_H)F} = \frac{0.059}{1-\alpha_H} \tag{14.31}$$

$\phi_{HS}^N$ is the Nernst potential of hydrogen (Eq (14.5)) at the surface:

$$\phi_{HS}^N = 0.059 \log\left([H^+]_s / p_{H2}^{1/2}\right) = 0.059 \log\left([H^+]_s / [H^+]_b\right) + \phi_{Hb}^N \tag{14.32}$$

and $\phi_{Hb}^N$ is the Nernst potential of the bulk hydrogen (first equality of above equation with subscript S replaced by b). This potential governs $i_{cH}$ in the absence of a mass-transfer limitation, or when $[H^+]_s = [H^+]_b$.

Equating $i_{MT}$ from Eq (14.30) with $i_{cH}$ from Eq (14.31) yields:

$$\log\left(\frac{k_{MT}F[H^+]_b}{10^3 i_{oH}}\right) + \log\left(1 - \frac{[H^+]_s}{[H^+]_b}\right) = -\frac{(\phi - \phi_{HS}^N)}{\beta_{cH}} = -\frac{(\phi - \phi_{Hb}^N)}{\beta_{cH}} + \frac{0.059}{\beta_{cH}} \log\left(\frac{[H^+]_s}{[H^+]_b}\right) \tag{14.33}$$

The factor of $10^3$ in the first term converts molar concentration from moles/liter to moles/cm$^3$. In order to draw a Tafel graph for the cathodic $H^+/H_2$ half cell, $k_{MT}$ and $[H^+]_b$ are fixed and at each potential difference $\phi - \phi_{Hb}^N$, Eq (14.33) is solved for $[H^+]_s/[H^+]_b$. Then the cathodic current $i_{cH} = i_{MT}$ is obtained from either Eq (14.30) or Eq (14.31). As shown in the following example, the above method gives the Tafel plot of $\phi - \phi_{Hb}^N$ Vs log(i).

<u>Example #5: Cathodic polarization with mass-transfer limitation</u>
Equation (14.22) is best handled nondimensionally:

$$S = \frac{k_{MT}F[H^+]_b}{10^3 i_{oH}} \quad x = \frac{[H^+]_s}{[H^+]_b} \quad Y = -\frac{(\phi - \phi_{Hb}^N)}{\beta_{cH}} \qquad \frac{0.059}{\beta_{cH}} = 1 - \alpha_H \tag{14.34}$$

which converts Eq (14.33) to:

$$\log S - Y = \log\left(\frac{x^{1-\alpha_H}}{1-x}\right) \tag{14.35}$$

S and $\alpha_H$ are input properties. For a series of Y values, Eq(14.35) is solved for x which is then inserted into the dimensionless version of Eq (14.30) in which $i = i_{MT}$ :

$$log\left(i / i_{oH}\right) = logS + log\left(1-x\right) \tag{14.36}$$

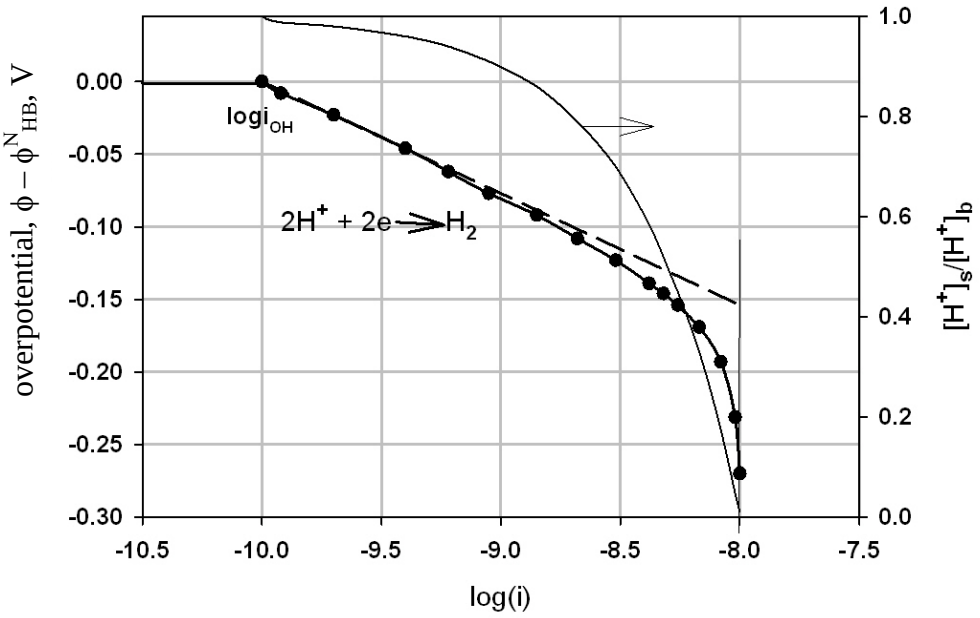


**Fig. 14.10 Cathodic polarization curve with concentration polarization**

Figure 14.10 is a plot of overpotential vs corrosion current from Eqs (14.30) and (14.35) for $\alpha_H = 0.23$ and S = 100. The curve starts without mass-transfer limitation, so the dashed line is the cathodic line in Fig. 14.6. The upper curve shows how $[H^+]_s$ decreases as the potential becomes increasingly negative thereby driving up the current.

The current reaches a limiting value $i_L$ when the surface concentration vanishes (x = 0). From Eq (14.30) the limiting current is:

$$i_{Lc} = \frac{k_{MT} F [H^+]_b}{10^3} \tag{14.37}$$

Anodic Tafel lines are also susceptible to limitation by mass transfer of the corroding metal ion from the surface to the bulk liquid. In general, the anodic limiting current $i_{La}$ is not equal to the cathodic value $i_{Lc}$.

### 14.4.10 Tafel diagrams with passivation

Figure 14.11 is a sketch of a realistic Tafel diagram for a metal like iron. Three regions of cathodic polarization curves are depicted. In the bottom of the sketch is the active corrosion region (line 3), which has been the sole mechanism dealt with up to this point. Line No. 3 assumes that the cathodic reaction is $2H^+ + 2e^- \rightarrow H_2$ with the Nernst potential given by Eq. (14.23). If $p_{H2}$ = 1 atm, $\phi^N_{H3}$ = - pH.

Active corrosion ends at the peak of the anodic curve, for which the coordinates are the *critical current density* $i_{crit}$ and the *passivation potential* $\phi_{pass}$. This occurs at the onset of formation of an oxide or hydroxide scale on the metal. Connection to Tafel diagrams is made by the half-cell reaction for the MO oxide:

$$MO + 2H^+ + 2e^- = M + H_2O$$

for which the passivation potential is:

$$\phi_{pass} = \phi^o_{pass} + 0.059 \log[H^+]^2 = \phi^o_{pass} - 0.118 pH$$

$\phi^o_{pass}$ is the standard electrode potential of the $MO/H^+$ half-cell.

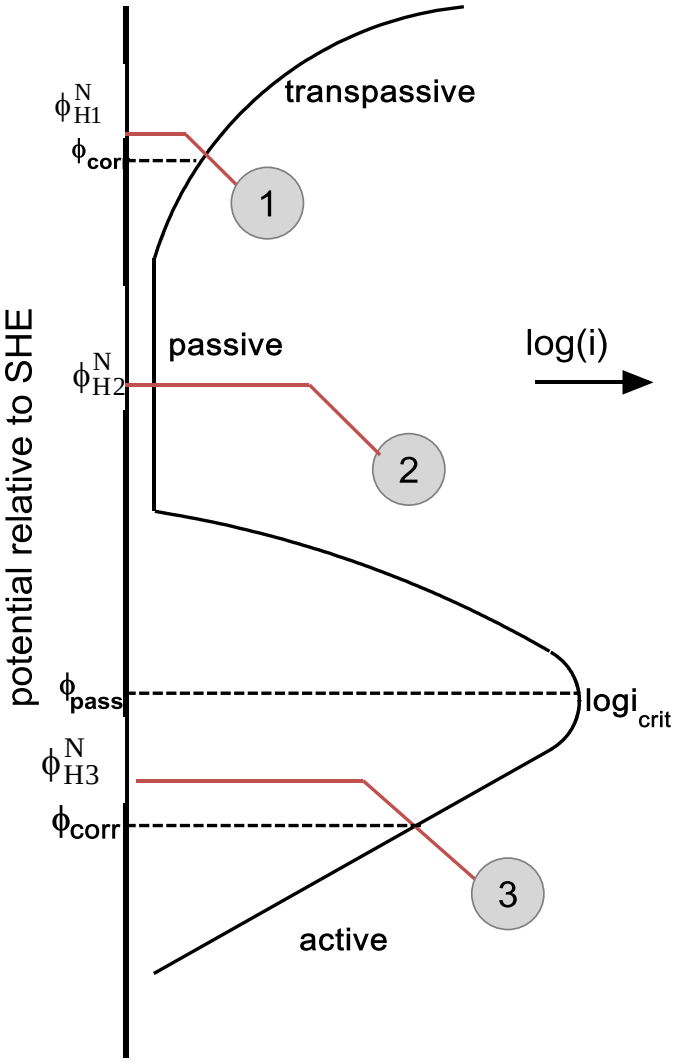


**14.11 Realistic anodic Tafel line for iron with three cathodic line intersections.**

When the $i_{crit}$ is reached, the anodic polarization curve rapidly decreases to the passive zone of very low corrosion rate (line 2).

At higher potentials the transpassive portion is attained, where the corrosion rate again increases with potential. In oxygenated solutions the cathodic reaction $½O_2 + 2H^+ + 2e \rightarrow H_2O$ (line 3) replaces the cathodic $H^+/H_2$ half-cell reaction in location No. 1 of Fig. 14.11.

Semi-quantitative forms of the anodic polarization curves for iron and stainless steel are shown in Fig. 14.12. Stainless steel is represented by chromium, which is the primary chemical actor for the surface of this alloy in water. Despite the general chemical similarity of Fe and Cr, their anodic polarization curves are not at all similar. The primary difference is the critical current densities of the two metals. The very large value of $i_{crit}$(Fe) make iron very difficult to passivate. The potential corresponding to the critical current density of Cr is an order-of-magnitude lower than that of Fe, which also makes the former easier to passsivate. This difference in corrosion

behavior between the two metals is the reason that the iron age morphed into the age of stainless steel and chrome plating.

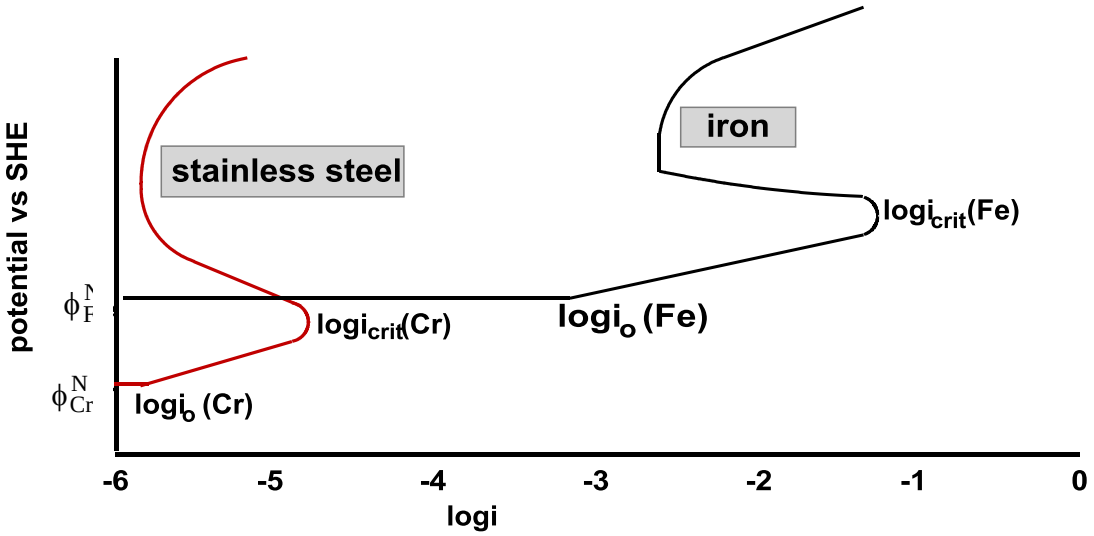


**Fig. 14.12 The anodic polarization curves of iron and chromium (stainless steel)**

## 14.5 Scales on structural metals

The initial reaction product of pure iron with water is the hydroxide, $Fe(OH)_2$. This compound further reacts with $H_2O$ and non-protective rust-colored $Fe(OH)_3$ is eventually produced. The poor properties of this corrosion product render pure iron an undesirable structural member if exposed to water.

### 14.5.1 Corrosion-product Properties

By structural metals we mean the iron-nickel-chromium alloys which provide the majority of the high-strength, elastic support of modern society's edifices. Nearly all of these applications exist at ambient temperatures, with the notable exceptions of fossil-fired and nuclear power plants, where temperatures up to 850$^o$C are involved. The compositions of three common alloys are listed in Table 14.2. There is a goodly spread in the compositions and the table gives rough averages. These alloys have somewhat different corrosion resistances to water and different strength versus temperature dependences. In what follows, mainly the properties of stainless steel are reviewed.

The result of metal corrosion in water (or air) are oxide *scales*, which are also called *films* or *barriers*. When a nearly-pure alloy such as Zircaloy corrodes, a single oxide scale is formed (Sect. 28.3.4). Stainless steel corrosion in ambient-temperature water, which is very slow, results in a two-layer scale, which is seen in Fig. 14.13.

**Table 14.2 Compositions of Fe, Cr, Ni alloys**

| Alloy | Ni % | Cr % | Fe% |
|---|---|---|---|
| stainless steel$^+$ | 10 | 18 | 72 |
| Inconel 600 | 76 | 16 | 8 |
| Inconel 625* | 68 | 21 | 5 |

$^*$(304 & 316)

*balance Mo, Ta

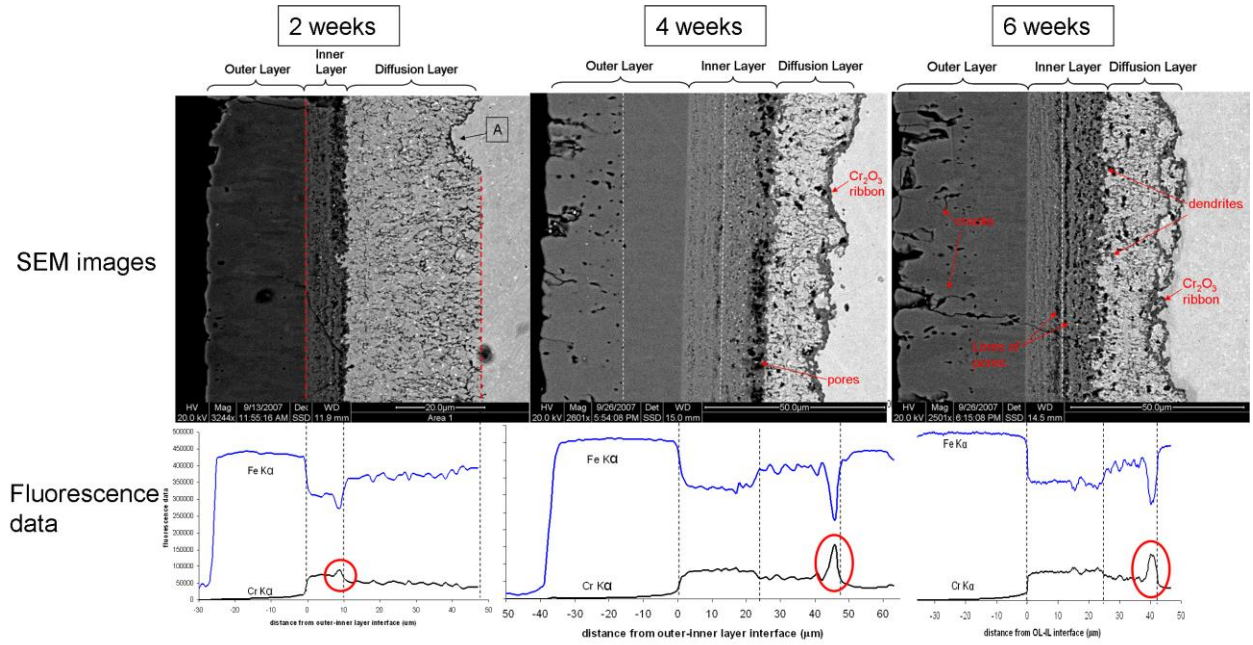


**Fig 14.13 Scanning electron micrographs of a multi-layer corrosion scale on steel exposed to supercritical water at 600 C and corresponding fluorescence spectra of Fe and Cr. The outer layer if $Fe_3O_4$, while the inner layer has a large percentage of spinel ($Fe,Cr_2O_4$). A "diffusion layer" is also seen which develops into a $Cr_2O_3$ ribbon after 4 weeks. [14]**

The outer layer of $Fe_3O_4$ is formed b outward migration of Fe, whereas the inner layer is formed by oxygen ion ingress. The boundary between the two is the original specimen surface. A material balance indicates that the amount of Fe lost The egress of iron atoms from the inner layer to the outer layer is reflected in the vacancies seen in the inner layer. In the diffusion layer (also kinetically formed and thermodynamically unstable, diffusion of oxygen ions into the metal ahead of the oxide layer races ahead of the concentration necessary to form oxide. This is eventually stopped by the formation of a $Cr_2O_3$ layer which impedes further diffusion and slows down the overall corrosion reaction.

The actual corrosion layer (i.e, that which controls the growth rate) is either the inner layer which is rich in spinel or chromite layer, or in general an oxide rich in Cr. Lying on top of this corrosion barrier is a collection of particles rich in ferrite. These scales are a class of mixed double oxides $AB_2O_4$ called *spinels*, where A and B denote mixtures of Fe, Ni and Cr(Sect. 3.8.5). The sublayer Cr-rich spinel grows into the base metal while the ferrite chunks are deposited from the liquid as recrystallized particles. One reason for this difference is the lower diffusion coefficient of Cr relative to Fe and Ni, which causes the outer layer to be formed principally from egress of Fe ions, leaving behind vacancies, in a process akin to the Kirkendall effect (see middle picture of Fig. 14.13).

Example #6: The Davis-Besse Pressure Vessel Head Corrosion

The higher corrosion rate of low alloy steels relative to stainless steels was dramatically demonstrated in the Davis-Besse incident, in which a large section of a PWR vessel head was consumed by reaction with boric acid. The incident started with a steady leak of reactor coolant, consisting of high purity water with boric acid (inserted in the core as a burnable poison for reactivity control) through stress-corrosion cracks in the control rod drive mechanism penetration fittings (Figs. 14.14 and 14.15). Once the coolant leaked out, it caked on the outer surface if the pressure vessel head, under moist conditions favorable for corrosion attack. This corrosion proceeded over a period of several years, as it was hidden from casual inspection by the thermal insulation present on top of the vessel head.

Ultimately the corrosion was discovered when the reactor was shut down and the workers in removing the thermal insulation for inspection of the stress corrosion cracks found the control rod in question to be loose; further investigation showed that corrosion had created a huge hole on the vessel head. The corrosion only stopped when it reached the stainless steel liner on the inner surface of the head. The purpose of this liner is not structural (it is designed to prevent corrosion of the head from the high-pressure (15 MPa), high-temperature (300$^{o}$C) coolant water) it ended up holding the full reactor pressure and fortunately it did not fail. This gigantic hole is shown in Fig. 14.16.

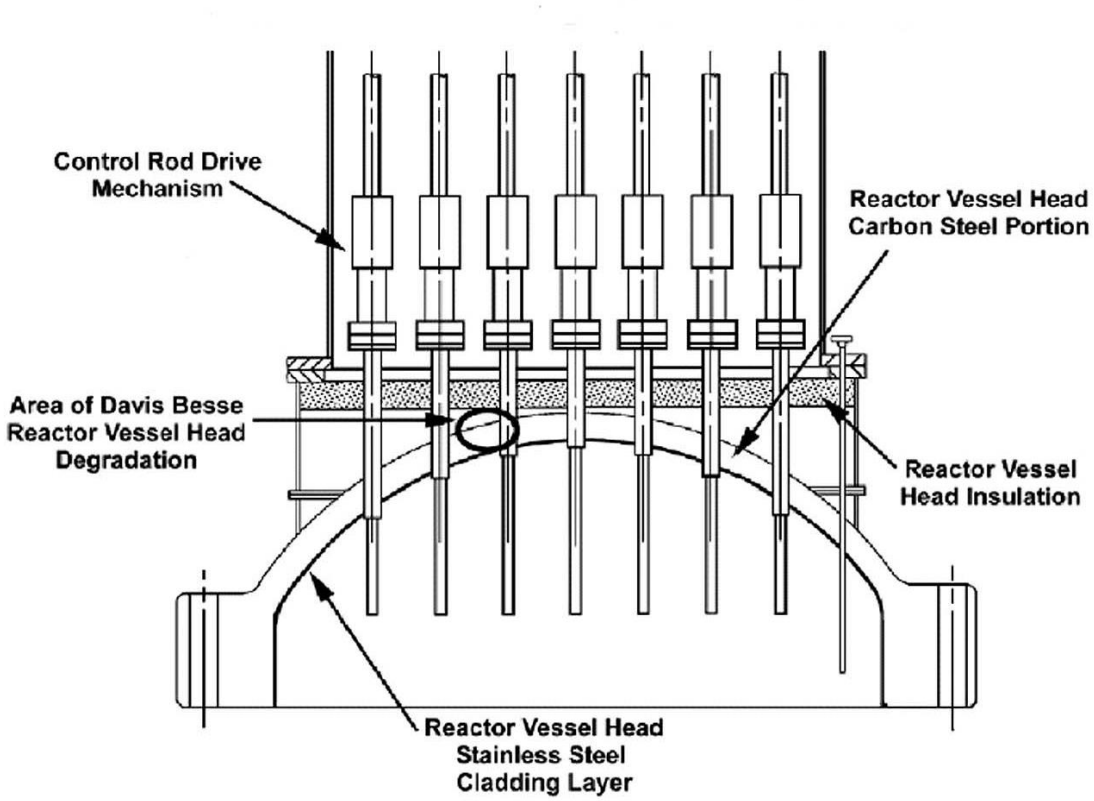


**Fig. 14.14 From Davis-Besse Reactor Vessel Head Degradation Lessons-Learned Task Force Report, September 20, 2002**

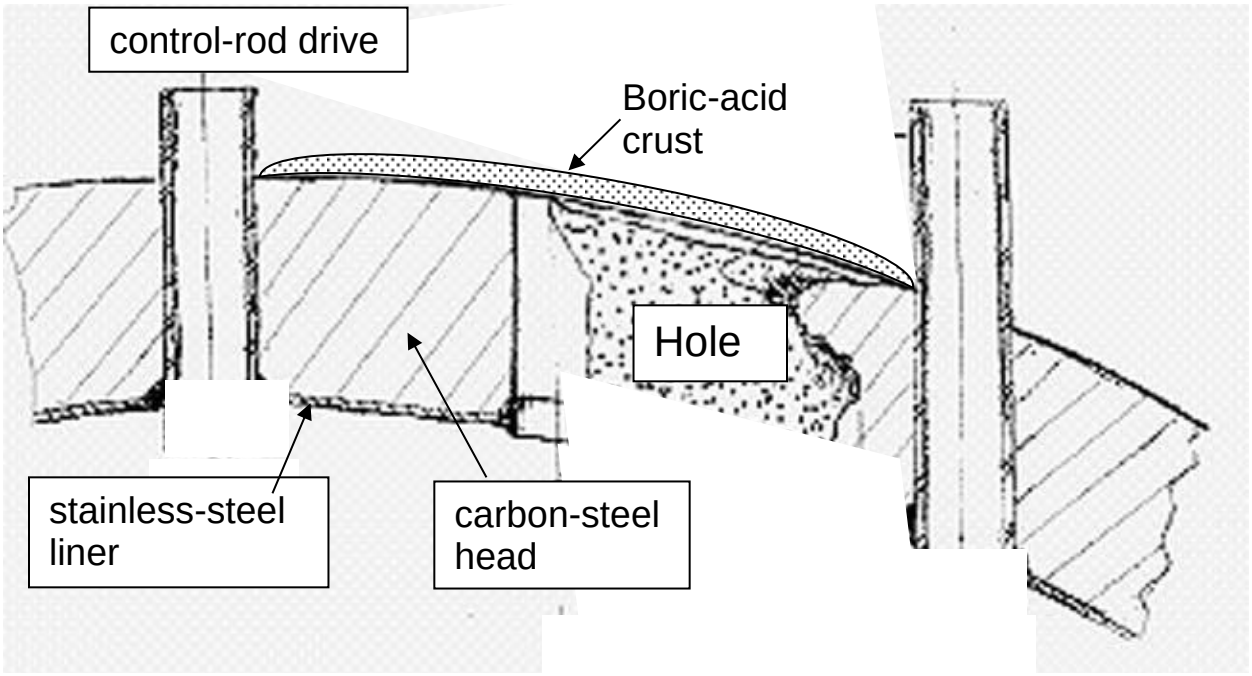


**Fig. 14.15 Corrosion attack from: Davis-Besse Reactor Vessel Head Degradation Lessons-Learned Task Force Report, September 20, 2002**

**Fig. 14.16 . Corrosion hole in the pressure-vessel head of the Davis-Besse reactor.**

### 14.5.2 Magnetite solubility in water

The spinel-structured nickel-chromium-iron oxides discussed in the preceding section are the most common corrosion films that form on the surfaces of piping in the primary circuit of LWRs. These oxides have a non-zero solubility in water and the metal ions dissolved at 300°C are carried through the primary circuit into the hot core. The solubility decreases with temperature so the metals can redeposit on the cladding as CRUD (Chalk River Undesirable Deposit). Consequently many papers, and even an entire book [6], have been devoted to understanding this problem. In the following, we derive the solubility of pure magnetite ($Fe_3O_4$, no nickel and chromium) from the thermodynamics of various iron compounds that constitute the dissolved metal. Sweeton and Baes [7] assume that the solubility is controlled by the following reactions:

$$\begin{aligned}
&\tfrac{1}{3}Fe_3O_4 + \tfrac{1}{3}H_2 + 2H^+ = Fe^{2+} + \tfrac{4}{3}H_2O \\
&\tfrac{1}{3}Fe_3O_4 + \tfrac{1}{3}H_2 + H^+ = Fe(OH)^+ + \tfrac{1}{3}H_2O \\
&\tfrac{1}{3}Fe_3O_4 + \tfrac{1}{3}H_2 = Fe(OH)_2 - \tfrac{2}{3}H_2O \\
&\tfrac{1}{3}Fe_3O_4 + \tfrac{1}{3}H_2 - H^+ = Fe(OH)_3^- - \tfrac{5}{3}H_2O
\end{aligned} \qquad (14.38)$$

For which the equilibrium expressions are:

$$K_0 = \frac{[Fe^{2+}]}{p_{H2}^{1/3}[H^+]^2} \qquad K_1 = \frac{[Fe(OH)^+]}{p_{H2}^{1/3}[H^+]} \qquad K_2 = \frac{[Fe(OH)_2]}{p_{H2}^{1/3}} \qquad K_3 = \frac{[Fe(OH)_3^-][H^+]}{p_{H2}^{1/3}} \quad (14.39)$$

If the water is pure (no added soluble acids or bases) and only $p_{H2}$ is specified, charge conservation gives:

$$\underline{\text{positive}} \qquad \underline{\text{negative}}$$
$$2[Fe^{2+}] + [Fe(OH)^+] + [H^+] = [Fe(OH)_3^-] + K_W/[H^+] \qquad (14.40)$$

The last term on the right-hand side is the $OH^-$ concentration, and $K_W$ is the water dissociation equilibrium constant ($K_W = [H^+][OH^-]$). Substituting Eqs (14.39) into (14.40) gives an equation from which $[H^+]$ can be determined (by trial and error).

At 300°C (typical LWR coolant temperature), the equilibrium constants are:

$$K_0 = 10^4 \qquad K_1 = 10^{-1} \qquad K_2 = 10^{-7} \qquad K_3 = 10^{-14} \qquad K_W = 10^{-11.2} \qquad (14.41)$$

Table 14.3 lists the solutions to the above equations for different $H_2$ pressures.

**Table 14.3 Magnetite solubility in 300°C pure water with added $H_2$**

| | | $[Fe(OH)_b^{2-b}]$, μ M | | | | | |
|---|---|---|---|---|---|---|---|
| $p_{H2}$, atm | pH | b = 0 | b = 1 | b = 2 | b = 3 | $[Fe_{tot}]$ | $\phi_H^N$ (V) |
| 0.1 | 5.62 | 0.027 | 0.11 | 0.05 | 0.002 | 0.19 | - 0.30 |
| 1 | 5.63 | 0.055 | 0.23 | 0.10 | 0.004 | 0.39 | - 0.33 |
| 10 | 5.66 | 0.103 | 0.47 | 0.22 | 0.010 | 0.80 | - 0.36 |

The table shows that for each factor of 10 increase in $p_{H2}$:

- the total Fe concentration doubles.
- the water electrochemical potential (last column) decreases by 10%
- the pH is practically unaffected

Most significant is the very low metal solubility; $[Fe]_{tot}$ is less than $10^{-6}$ moles per liter. This accounts for the stability of magnetite in water.

The effect of temperature on magnetite solubility in water is a crucial property that determines in-core behavior. This effect is shown in Table 14.4.

**Table 14.4 Magnetite solubility in neutral water as a function of temperature**

| Temp., °C | $[Fe_{tot}]$, μM |
|---|---|
| 100 | 4.0 |
| 200 | 1.5 |
| 300 | 0.3 |

The numbers in Table 14.4 indicate that precipitation of Fe, Ni, Cr oxides on the hot fuel cladding (T > 350°C) is inevitable.

### 14.5.3 Oxide scale on a divalent metal

The reason for choosing a divalent metal for explaining aqueous corrosion is to keep the notation simple. The oxide formula is $MO_{1-y}$ where y = 1 – O/M is the hypostoichiometry factor. This parameter is equal to the fraction of vacant anion lattice sites.

There are two mechanisms by which a metal oxidizes:

i) metal ions migrate from the metal/scale interface to the scale/solution interface where the ions are converted to an oxide by reaction with $H_2O$ or $O_2$ dissolved in water.

ii) oxygen ions produced at the scale-solution interface diffuse through the scale to the metal-scale interface where they extract metal atoms and convert them to the oxide.

Only the second of these possibilities is considered in what follows.

A schematic phase diagram of the M-O binary system is given in Fig. 14.14 The oxide scale

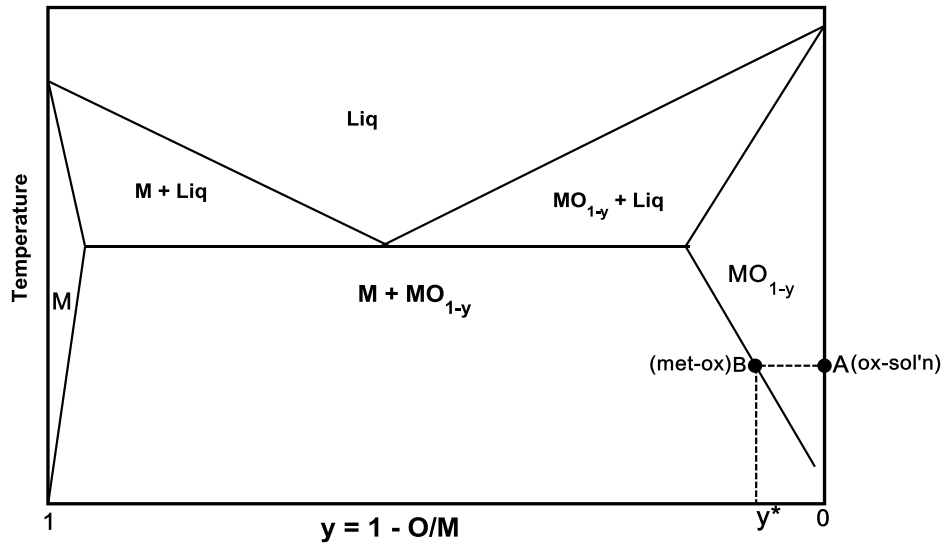


**Fig. 14.17 Phase diagram of the M-O metal/oxygen system**

that forms on the metal substrate has bounding interfaces at points A and B. The aqueous solution maintains the outer surface of the oxide (point A) perfectly stoichiometric, or M/O = 1, y = 0. The oxide contacting the metal (point B) is $MO_{1-y^*}$, where y* is the stoichiometry factor of the oxide in equilibrium with the metal.

Figure 14.17 shows the metal in contact with the oxidizing solution with the oxide scale separating the two. The location x = 0 in Fig. 14.18 is equivalent to point B in Fig. 14.17, and x = L corresponds to point A.

If anions are missing but all cation sites are filled (as assumed here), electrical neutrality is maintained by the two electrons formerly associated with the metal atom that has been oxidized to $M^{2+}$. Where do these electrons go? As shown in Fig. 14.18, they move to the oxide/solution surface where they reduce neutral oxygen in the solution to anions ($O^{2-}$). The electron flux is assumed to be sufficiently rapid such that local electrical neutrality is maintained throughout the oxide (there are no emergence of space charges in the oxide). Basically, $c_e = 2c_{VO}$ everywhere in the oxide.

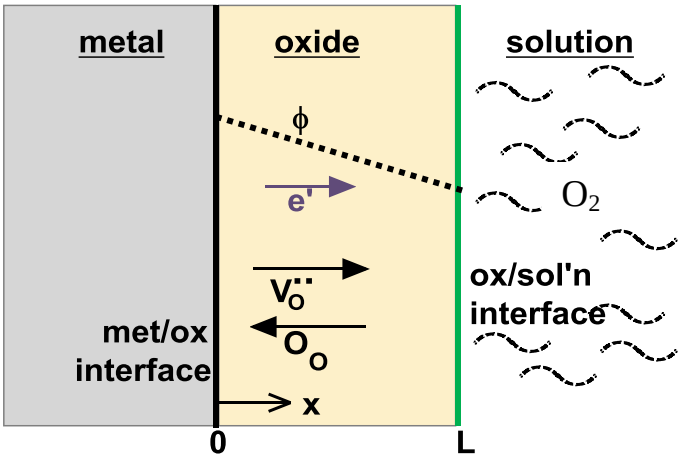


**Fig 14.18 Schematic of a metal with an oxide scale immersed in an aqueous solution**

Oxygen ions migrate by the vacancy mechanism (Sect. 5.4), which means that the flux of oxygen ions through the oxide can equally well be considered to be movement of anion vacancies in the opposite direction:

$$J_O = -J_{VO} \qquad (14.42)$$

This illustrative corrosion mechanism can be described by the following electronic processes:

1. at <u>the metal/oxide-scale interface</u> (x = 0): $M(met) \rightarrow M_M + V_O^{\cdot\cdot}(met/ox) + 2e'\ (met/ox)$

2. <u>in the oxide scale:</u> e' (met/ox) $\rightarrow$ e' (ox/sol'n)
and $V_O^{\cdot\cdot}(met/ox) \rightarrow V_O^{\cdot\cdot}(sol'n/ox)$

3. <u>at the oxide-scale/sol'n interface</u> (x = L):

$$\tfrac{1}{2}O_2(sol'n) + 2e'(ox/sol'n) + V_O^{\cdot\cdot}(ox/sol'n) \rightarrow O_O(ox/sol'n)$$

---

*Kroger-Vink notation*
Identification of the defects in the above reactions follows *Kroger-Vink* notation (see Chapter 4, Sect. 4.3.2). In this method, the letter signifies the type of defect: V for vacancy, I for interstitial. The subscript indicates the location of the entity: O means the anion (oxygen) sublattice, M means the cation (metal) sublattice, etc. The superscript indicates the charge deviation from the perfect lattice, dot $\cdot$ for positive charge and apostrophe ' for negative charge. Accordingly, the symbol $V_O^{\cdot\cdot}$ in the above reactions and in Fig. 14.18 identifies a vacancy (V) on the anion sublattice (sub O) which is doubly-<u>positively</u>-charged relative to the same site occupied by an oxygen ion. e' symbolizes an electron with a single negative charge. A missing charge symbol indicates species on normal lattice positions ($M_M$ means a cation on the cation sublattice and $O_O$ denotes an anion on the anion sublattice). The terms in parentheses give the macroscopic location of the species.

---

The actual mechanism of the interface reaction is more complex than the simple process shown here. Whatever the mechanism the overall corrosion reaction in this example is

$$M(met) + \tfrac{1}{2}O_2(sol'n) = M_M + O_O$$

The remaining question is how the anion vacancies are produced at the metal/oxide interface. The explanation is twofold: i) the $O^{2-}$ anions move by hopping into existing vacant anion sites, which are those moving in the opposite direction, as explained in the previous paragraph; ii) the very act of creating $M^{2+}$ cations in the oxide lattice structure automatically creates vacant anion sites in order to preserve the crystal structure. This step is illustrated in Fig. 14.19, where again for the purpose of illustration, the MO crystal is assumed to be the NaCl-type (Fig. 2.9).

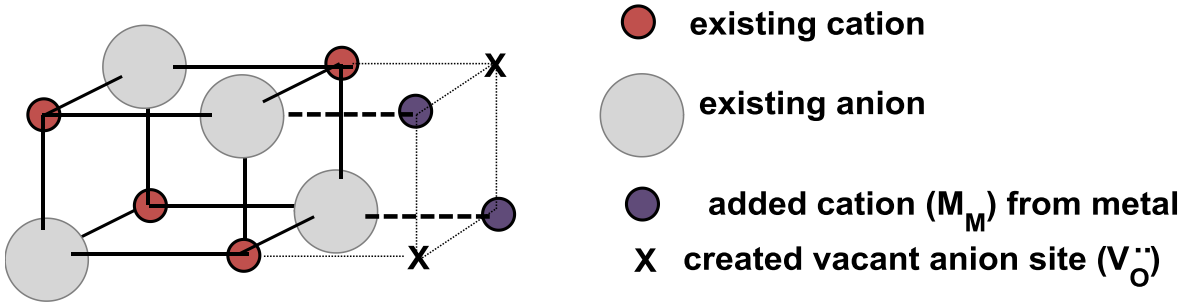


**Fig. 14.19 anion vacancies created by conversion of metal atom to metal ion in oxide**

The objective of the following analyses is to calculate the flux of oxygen vacancies that is responsible for growth of the scale. The rate of scale growth is determined from:

$$\frac{dL}{dt} = \frac{J_{VO}}{c_M} \tag{14.43}$$

where $c_M$ is the molar density of the cations in MO, which is equal to the anion-site concentration. Once $J_{VO}$ is known as a function of L, Eq (14.43) can be integrated to give L = f(t).

### 14.5.4 Flux through the oxide scale

The flux of oxygen vacancies (mole/cm$^2$-s) through the corrosion layer is driven by two gradients:

- The *concentration gradient*, according to Fick's law:

$$J_{conc} = -D_{VO}\frac{dc_{VO}}{dx} \tag{14.44}$$

- The *electric potential* gradient acts on the positively-charged vacancies:

$$J_{elec} = -u_{VO}c_{VO}\frac{d\phi}{dx} \tag{14.45}$$

where $c_{VO}$ is the anion vacancy concentration (moles per unit volume) and $\phi$ is the *electric potential*, which is expressed in terms of the *electric field* (Volts/cm):

$$E = -\frac{d\phi}{dx} \tag{14.46}$$

and the relation of mobility ($u_{FO}$) to diffusivity ($D_{VO}$):

$$u_{VO} = \frac{z_{VO}F}{RT}D_{VO} \tag{14.46}$$

$u_{VO}$ is the mobility of oxygen vacancies in the oxide (units of $cm^2$/Volt-s). $z_{VO}$ = +2 is the charge on anion vacancies (relative to the perfect lattice, Kroger-Vink notation). **F** is the Faraday (96.5 kJ/mole-Volt)

The total oxygen vacancy flux is the sum of the two contributions:

$$J_{VO} = -D_{VO}\frac{dc_{VO}}{dx} + u_{VO}c_{VO}E \tag{14.47}$$

---

Sign of E

Thermodynamically, oxidation of a metal is favored if the potential $\phi$ is positive (see Fig. 14.1). Similarly, corrosion kinetics are accelerated by a positive potential of the metal relative to that of the solution, as seen by the dashed line in Fig. 14.15. With the distance x positive in the direction shown in the figure, the slope of $\phi$ is negative, so that by Eq (14.45) $J_{elec}$ is positive and by Eq (14.46), E is positive.

---

Calculation of the rate of scale growth requires two integrations:

1. of Eq (14.47) over $0 < x < L$ to obtain $J_{VO}(L)$
2. of Eq (14.43) to determine L(t).

### 14.5.5 Position-independent electric field

Integration of Eq (14.47)

At steady-state, $J_{VO}$ is constant throughout the oxide, and provided that the electric field E does not depend on x, Eq (14.47) can be integrated .

In non-dimensional form, the flux equation (Eq (14.48)) is:

$$\frac{1}{\omega}\frac{d\,y}{d\,\eta} - y = -\Sigma \tag{14.48}$$

where

$$y = \frac{c_{VO}}{c_M} \qquad \eta = \frac{x}{L} \qquad \omega = \lambda \times L \times E \qquad \Sigma = \frac{J_{VO}}{\lambda \times c_M \times D_{VO} \times E} \qquad \lambda = \frac{z_{VO}F}{RT} \tag{14.49}$$

The conditions at the extremities of the scale are:

$$y = y^* at\ \eta = 0\ \left(scale/metal\ interface\right) \tag{14.50}$$

$$y = 0 at\ \eta = 1\ \left(scale/sol'n\ interface\right) \tag{14.51}$$

The solution of Eq (14.48) subject to Eq (14.50):

$$\frac{\Sigma - y}{\Sigma - y^*} = e^{\omega\eta} \tag{14.52}$$

y* is the dimensionless oxygen vacancy concentration in the scale at the scale/metal interface. Application of Eq (14.51) yields the dimensionless form of the vacancy flux:

$$\Sigma = \frac{y^*}{1-e^{-\omega}} \tag{14.53}$$

To return this formulation of the vacancy flux to physical reality, we take the limiting cases:

E $\rightarrow$ 0, or by Eq (14.49), $\omega \rightarrow 0$; Eq (14.53) reduces to $\Sigma = y^*/\omega$, or using Eq (14.49)

$$J_{VO} = D_{VO}\left(c_M y^*\right)/L \tag{14.54}$$

:

which is the integrated form of the first term of Eq (14.47).

E $\rightarrow \infty$, or by Eq (14.49), $\omega \rightarrow \infty$; Eq (14.53) reduces to $\Sigma = y^*$, or using Eq (14.49):

$$J_{VO} = u_{VO}\left(c_M y^*\right)E \tag{14.55}$$

which is the integral of the second term of Eq (14.47).

Substituting $J_{VO}$ in terms of $\Sigma$ from Eq (14.49) into Eq (14.43) using Eq (14.53) for $\Sigma$ gives:

$$\frac{dL}{dt} = D_{VO}y^*\left(\frac{\omega}{1-e^{-\omega}}\right)\frac{1}{L} \tag{14.56}$$

Integration of Eq (14.56)

E was taken to be constant with x in deriving Eq (14.56) but time-integration hinges on how the electric field varies with L . Integrating Eq (14.46) with constant E gives:

$$E = \frac{\phi_M - \phi_S}{L} = \frac{\Delta\phi}{L} \tag{14.57}$$

The electric potential difference ($\Delta\phi$) is a property of the metal ($\phi_M$) and the solution ($\phi_S$) , and is supposed to be independent of scale thickness. As a result, E×L is constant, and from Eq (14.49), $\omega = \lambda \times \Delta\phi$.

Integrating Eq (14.56) with L = 0 at t = 0:

$$L^2 = \left[2D_{VO}y^*\left(\frac{\lambda\Delta\phi}{1-e^{-\lambda\Delta\phi}}\right)\right]\times t \tag{14.58}$$

yields the parabolic growth law but with a rate coefficient that differs from that for purely diffusion control by the factor in parentheses in Eq (14.58). This "potential-modification factor" is shown in Fig. 14.20. At a typical LWR primary water temperature of 300°C ($\lambda$ = 36), a metal-solution potential difference of ¼ V increases the corrosion rate by a factor of 10.

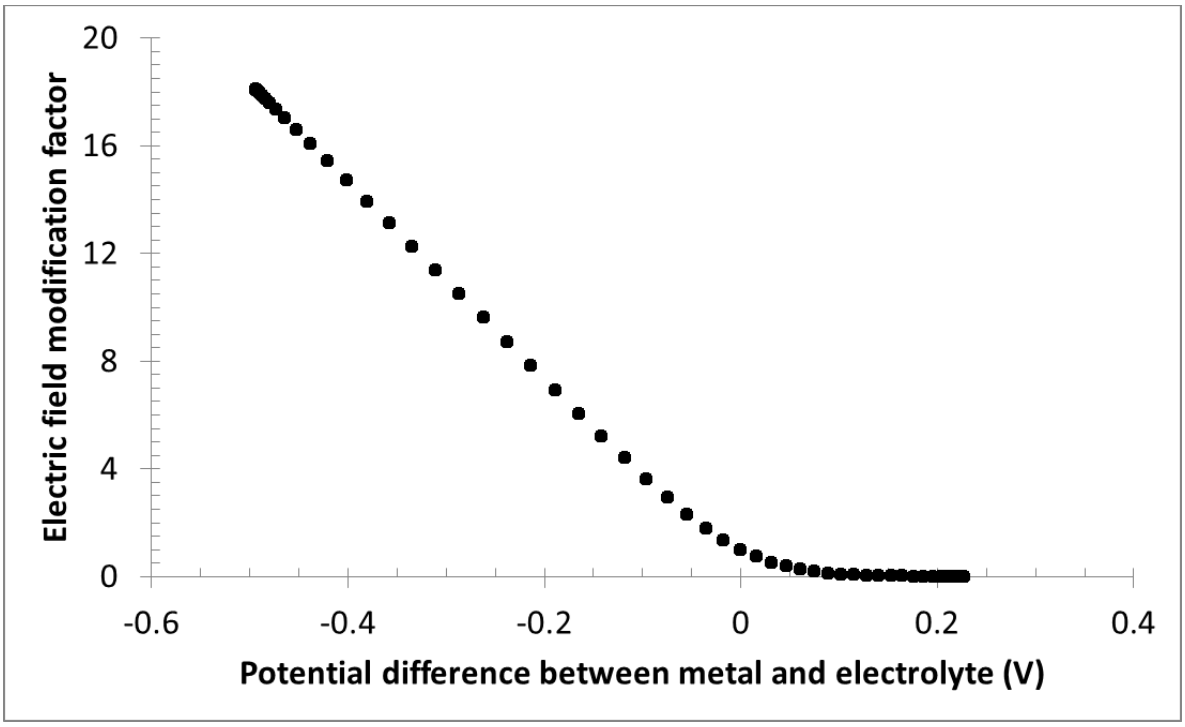


**Fig. 14.20 Factor by which the parabolic scaling rate is increased by the metal-solution electric potential difference (Ref. 13)**

### 14.5.6 Space charge in the oxide scale

If the electric potential does not vary linearly through the scale, as shown in Fig. 14.18, the analysis is considerably more complex.

To avoid charge buildup, the net charge flux at any point in the scale must be zero, or:

$$J_e = 2J_{VO} \tag{14.59}$$

where $J_e$ is the electron flux:

$$J_e = - D_e \frac{dc_e}{dx} + u_e c_e E \tag{14.60}$$

Although the net charge flux is zero, sections of the oxide scale perpendicular to the interfaces may build up a steady-state net electrical charge, which generates an electric-field gradient by *Poisson's equation:*

$$\frac{dE}{dx} = \frac{F}{\varepsilon^*}(2c_{VO} - c_e) \tag{14.61}$$

$\varepsilon^*$ is the permittivity of the oxide, ~$10^{-12}$ Coulomb/Volt-cm. The term in parentheses is the *space charge* (units of Coulombs/cm$^3$); even though the electron and anion vacancy fluxes are related by Eq(14.59) the two concentrations do <u>not</u> follow $c_e = 2c_{VO}$.

Integration of Eqs (14.47), (14.60), (14.61)
These three coupled first-order ordinary differential equations require boundary conditions, which for anion vacancies are the same as in Eq(14.50) (with y = $c_{VO}/c_M$).
$c_e(x)$ and E(x) need to be specified at x = 0.
As in the preceding section, L is regarded as a constant for these integrations.

What remains to be specified is a solution method, which is inevitably numerical. Dimensionless dependent variables are:

$$q_{VO} = / \, dc_{VO} \, \mathrm{L}^2 \qquad q_e = / \, dc_e \, L^2 \qquad w = / \, \mathrm{EL} \tag{14.62}$$

The constants λ and δ in the above definitions are:

$$\lambda = \frac{2\mathrm{F}}{\mathrm{RT}} = 36 \, Volt^{-1} \text{ at room temperature} \qquad \delta = \frac{F}{\varepsilon^*} = \frac{96,500}{9\times10^{-13}} = 1.1\times10^{17} \, \frac{Volt - cm}{mole} \tag{14.63}$$

The dimensionless forms of the anion-vacancy flux through the oxide scale and its thickness are:

$$j = \frac{\lambda\delta}{D_{VO}} \mathrm{L}^3 \mathrm{J}_{\mathrm{VO}} \qquad \eta = \frac{\mathrm{x}}{\mathrm{L}} \tag{14.64}$$

In terms of the above dimensionless variables, Eqs (14.47), (14.60), and (14.61) are

$$j = - \frac{dq_{VO}}{dh} + wq_{VO} \tag{14.65}$$

$$4j = - \frac{dq_e}{dh} - 1/2(wq_e) \tag{14.66}$$

$$dw/dh = 2q_{VO} - q_e \tag{14.67}$$

The factor of 4 in Eq(14.66) is twice the ratio $D_{VO}/D_e$, with the diffusivities estimated by Fromhold [8]. It also invokes Eq (14.59).

The boundary conditions for Eq (14.65) are:

$$\theta_{VO}(0) = \lambda\delta c_M \mathrm{y}^* \mathrm{L}^2 \qquad \theta_{VO}(1) = 0 \tag{14.68}$$

/where y* is the nonstoichiometry parameter characterizing the oxide at the metal/oxide interface (Fig. 14.14). For the system studied in Ref. 8, the concentration at this location is $y^* = 4\times10^{-6}$ . When inserted into the first equality of Eqs (14.69) the bounding condition on the anion vacancy concentrations is:

$$q_{VO}(0) = (36)(1.1\times10^{17})(0.15)(4\times10^{-6})(10^{-14})L^2 = 0.02L^2 \tag{14.69}$$

The oxide scale thickness L is in nanometers. 0.15 is the molar density of NiO (a typical MO oxide). The factor of $10^{-14}$ converts $nm^2$ to $cm^2$.

The electron concentration in the oxide at the interface with the metal is not known, so the condition for Eq (14.66) at $\eta = 0$ needs to be treated as an undetermined condition.

Finally, the $\eta = 0$ condition for Eq (14.67) requires knowledge of $E_o$, which depends on the separation of charges between the metal and the oxide at their common interface. There is no *a priori* method of assessing this quantity, although several sources give $E_o \sim 10^5 - 10^6$ V/cm. Once a value of this parameter is specified, the boundary condition for Eq (14.67) is:

$$w(0) = / E_o L \tag{14.70}$$

Solution of the three coupled ordinary differential equations is accomplished numerically (e.g., trial-and-error, finite difference). Figure 14.21 shows the spatial distributions of the three properties that characterize a 3.3 nm-thick oxide scale. The anion-vacancy concentration ($c_{VO}/c_M$) decreases slowly from the oxide/metal interface ($\eta = 0$) to the oxide/solution interface ($\eta = 1$).

**Fig. 14.21 Variation of the concentrations of the anion vacancies and electrons and of the electric field with position in the scale. L = 3.3 nm** $D_{VO} = 4\times10^{-11}$ cm$^2$/s at 300 K.

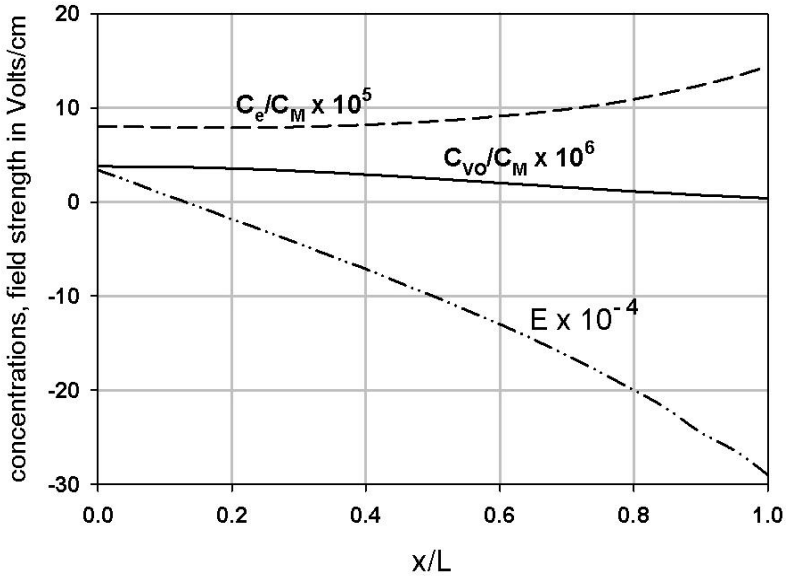


The important feature of this plot is the substantial variation of the electric field E with distance through the scale. According to Eq (14.61), this feature is responsible for the space charge in the oxide, which is caused by the difference in $c_e/c_M$ and $c_{VO}/c_M$ curves in Fig. 14.21.

$J_{VO}$ and the other two parameters are shown in Table 14.5 for four values of the scale thickness L.

**Table 14.5 parameters in the oxide at the metal/oxide interface for various scale thicknesses**

| L, nm | $J_{VO}$ x $10^{11}$ moles/cm$^2$-s | $c_e(0)/c_M$ × $10^5$ | $E_o$, V/cm × $10^{-4}$ |
|---|---|---|---|
| 3.3 | 1.6 ± 0.4 | 5.0 ± 2.3 | 2.2 ± 3.9 |
| 5.0 | 0.75 ± 0.3 | 4.8 ± 0.3 | 2.6 ± 1.0 |
| 7.5 | 0.22 ± 0.04 | 3.3 ± 0.3 | 3.1 ± 0.8 |
| 10.0 | 0.07 ± 0.02 | 3.5 ± 0.5 | 7.2 ± 1.7 |

The fitted values of the electron concentration at x = 0 (3rd column) are very close to Fromhold's guess [8]. The metal/oxide interface electric field $E_o$ is below the commonly-reported value of $10^5$-$10^6$ Volt/cm essentially independent of scale thickness.

The initial values of the electron concentration and the electric field, on the other hand, are chosen as part of the random parameter-search process. The electron concentration at x = 0 ($E_o$) is very close to the value suggested by Fromhold [8]. Its x-variation, however, requires some explanation.

In order for electrons to move from the metal/oxide interface to the oxide/solution interface, Eq (14.60)suggests that the e' concentration gradient should be the opposite of that shown in Fig. 14.21; that is, the electrons are moving up instead of down their concentration gradient. The reason for this behavior is the strong coupling between Eqs (14.66) and (14.67);

- $\theta_e$ starts out about an order-of-magnitude larger than $\theta_{VO}$, so that the latter can be neglected in Eq (14.67): $d\omega/d\eta \approx -\theta_e$
- the gradient of the electric field $\omega$(or E in dimensional terms, see Eq (14.63)) is always negative and $\omega < 0$.
- the gradient of $\theta_e$ becomes positive: $d\theta_e/d\eta > 0$

This feedback phenomenon is clearly evident in the two dashed curves in Fig. 14.21 and is observed for all scale thicknesses.

Integration of Eq (14.43)

With the dependence of the anion-vacancy flux $J_{VO}$ on scale thickness L summarized in Table 14.5, the time variation of scale growth is determined by integration of Eq (14.43):

$$L(nm) = 2.1 \times ln(3.6 \times 10^{-3} t + 1) \qquad (14.71)$$

t is in seconds. This equation is plotted in Fig. 14.22. For the anion-vacancy diffusivity assumed for this calculation ($D_{VO} = 4 \times 10^{-11}$ cm$^2$/s), a scale thickness of 10 nm is achieved in ~ 10 hours.

For comparison, a parabolic scale-growth curve from Eq (14.58) is also plotted in Fig. 14.22. The sharper bend of the solid curve more closely resembles experimental data for scales in the size range of the graph. The parabolic line in Fig. 14.21 is nearly everywhere greater than that of Eq (14.71) because of the inhibiting effect of the space-dependent electric field on the corrosion rate (second term of Eq (14.48)). The electric field line in Fig. 14.21 is negative over 90% of the scale thickness, so the second term in Eq (14.48) diminishes rather than increases the flux of anion vacancies from the metal/oxide interface to the oxide/solution interface. This is equivalent to reducing the flux of oxygen ions in the opposite direction, and hence decreasing the rate of oxide formation.

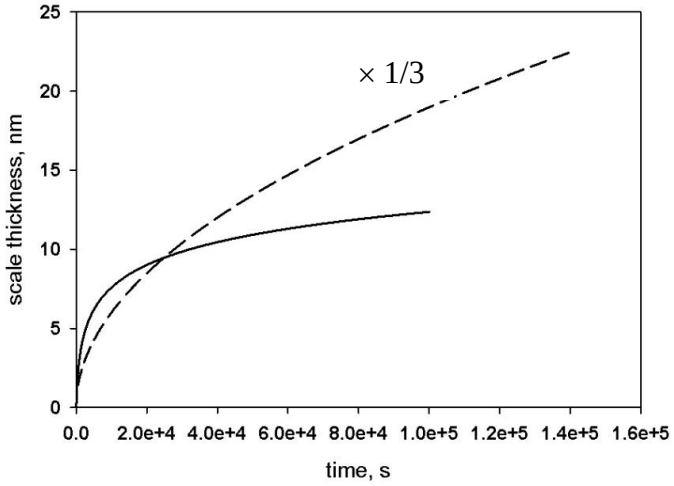


**Fig. 14.22 Scale growth according to Eq (14.71) (solid curve); parabolic growth Eq (14.58) (dashed line)**

## 14.5.7 Growth of passive scales

A scale forms on a metal when solution conditions (i.e., pH and potential) are in the passivity region of the polarization curve of Fig. 14.11. The film is called "passive" because it persists indefinitely and protects the metal from rapid corrosion. The phenomenon is important for structural metals, all of which, in air or water, should (thermodynamically) be converted back to the ore whence they originated. In particular, chemical immunity of aluminum, chromium and stainless steel from attack by water, even at high temperatures, is due to the formation of passive films. Because these scales are no more than a few nanometers thick, they can only be seen with appropriate microscopes (Fig. 14.13).

In an aqueous phase in an LWR, the electric potential of the metal structure and the coolant are determined by many factors that may not be controllable. In this case, scale growth (corrosion) and passivation are treated as kinetic phenomena. The mechanism is straightforward: A steady-state corrosion-oxide thickness is reached when the rate of scale growth at the metal/oxide interface equals the rate at which the oxide dissolves at the oxide/sol'n interface.

Dissolution is assumed to proceed at the solution/scale interface by the reaction:

$$MO + 2H^{+} \rightarrow M^{2+}(sol'n) + H_2O \qquad (14.72)$$

at a constant rate given by:

$$J_{diss} = k_{rxn}\left[H^+\right]^2, \quad moles/cm^2 s \tag{14.73}$$

where $k_{rxn}$ is the rate constant for the dissolution reaction Deposition of M by the reverse step of reaction Eq. (14.72) is neglected. This assumes that the $M^{2+}$ concentration in the water is well below the solubility limit (e.g., Sect. 14.5.2).

The scale achieves a steady-state thickness when:

$$J_{VO} = J_{diss} \tag{14.74}$$

The steady-state oxide-scale thickness is obtained from $J_{VO}$ and the model of the corrosion process, as analyzed in the previous section.

Example #7: Steady-state corrosion-scale thickness
A metal M for which the corrosion kinetics are listed in Table 14.5 is immersed in an aqueous solution of a specified pH. The rate constant of reaction (14.73) for a particular metal is $k_{rxn} = 2\times10^8 \cdot \frac{cm^4}{mole - s}$

(a) what is the steady-state oxide scale thickness in water of pH = 10?
From Eq (14.73), $J_{diss} = (2\times10^8)(10^{-10})^2 = 2\times10^{-12}$ moles/cm$^2$-s
From Table 14.5, $L_{SS} = 7.5$ nm

(b) Steady-state oxide scale thickness in water of pH = 7
From Eq (14.73), $J_{diss} = J_{VO} = (2\times10^8)(10^{70})^2 = 2\times10^{-6}$ moles/cm$^2$-s
The numbers in Table 14.5 are fitted to the equation :
$J_{VO}\times10^{11} = 57L^{-2.84}$ units: flux in moles/cm$^2$-s; thickness in nm
For the above value of $J_{VO}$, the equation gives $L_{SS} = 0.06$ nm, which is effectively a bare surface.

## 14.6 Pitting

Until now, only *uniform corrosion* has been treated. If this were the only form of electrochemical attack of metals, our industrial society would be relieved of a significant portion of its problems A particularly uncompromising form of attack is called *localized corrosion*. As the name implies dissolution of the metal occurs in isolated spots. Also, the direction of the process is into the, metal, rather than on its surface, which is the result of uniform corrosion. There are two distinct forms of localized corrosion, *pitting* and *crevice corrosion*. Even the piping of water-cooled nuclear reactors exposed to 300$^o$C exceptionally-clean water suffers from this problem.

### 14.6.1 Generalities

Pitting is initiated by penetration of the corrosion scale on the surface of the metal by one of three mechanisms:
**1**. movement of an aggressive anion (esp. $Cl^-$) through the passive scale by diffusion, without leaving macroscopic signs. This process is facilitated by high electric potential differences across the scale and/or a scale which is amorphous rather than crystalline

**2**. breakage of the passive scale by any one of a number of causes, including metal non-uniformities, grain boundaries, surface roughness which are mimicked by the scale. Weak points in the passive scale can progress to local rupture by temperature or stress changes of the component. Penetration of reactive anions initiates pit growth
**3**. adsorption of aggressive anions on the surface of the passive scale. The negative charge of the anions pulls metal ions from the inside of the film. In addition this mechanism tends to thin the scale locally, eventually forming an embryo pit.

There is no established theory of pit initiation or for pit growth. The reasons are twofold: first, the geometry of pits is so variable that no single shape fits; second, the diameter-to-depth ratio is near unity, which means that convection due to moving water influences their growth. These difficulties are illustrated by the large range of pits observed on metals that are shown in Fig.14.23.

In view of the enormous range of sizes and shapes and the complexity of the electrochemistry involved, it is no surprise that no quantitative modeling of the growth kinetics of pit corrosion exists. However, detailed qualitative accounts of pitting corrosion can be found in Ref. 2.

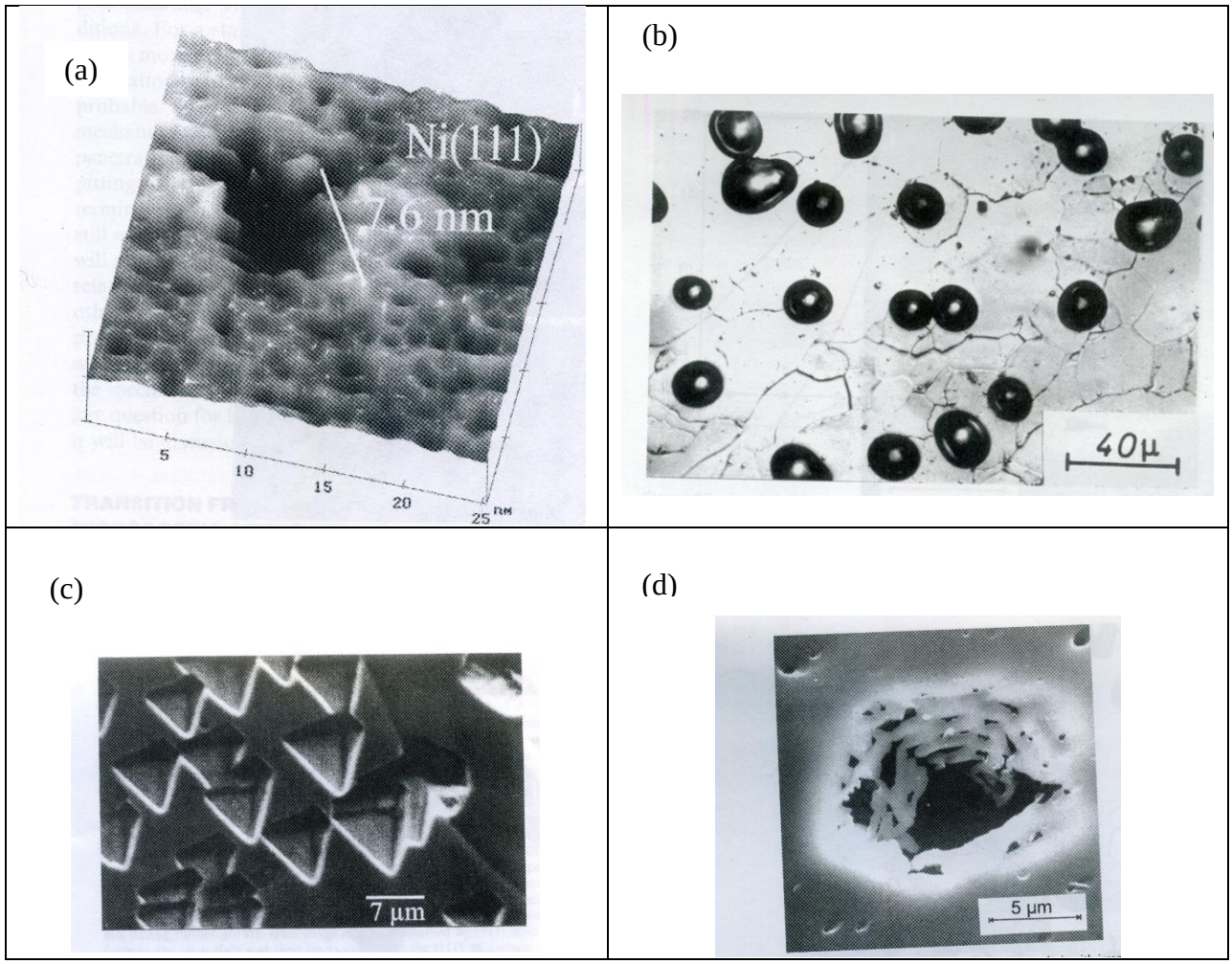


**Fig.14.23 Pits in metals (from Ref. 1). (a) Scanning-tunneling microscope image of a pit on single-crystal Ni in 0.2 M NaCl; (b) optical micrograph of pits on polycrystalline Fe in 0.1M $K_2SO_4$; (c) Scanning-electron micrograph of pits in polycrystalline Ni in 0.2 M NaCl; (d) Optical micrograph of a pit in polycrystalline Ni in 0.1 M $K_2SO_4$.**

## 14.7 Crevice corrosion

Crevice corrosion, a close cousin of pitting corrosion, occurs in geometrically simple confines, such as close-fitting metal parts that are purposely or accidentally exposed to water containing aggressive anions. Typical venues for crevice corrosion include bolts, valves, tube holders (as in steam generators) and welded joints. The flat sides of a crevice are usually the same metal and corrode much less aggressively than the bottom. Crevices can be formed from two dissimilar metals or with on side a metal and the other a nonmetal. An example of the latter is a gasket pressed against a flange. Cracks produced by stress-corrosion are treated as crevices for the purpose of calculating the composition of the solution at the crack tip (Chap. 25).

Contrary to the variety of irregular shapes of pits, the geometry of crevices is regular and so is a favorite target of corrosion modelers. Crevices are assigned a well-defined depth (L), a constant width (w), and a straight third dimension with no property or condition variations. The crevice opens to the bulk water at its mouth. Such a crevice in iron is shown in Fig. 14.24.

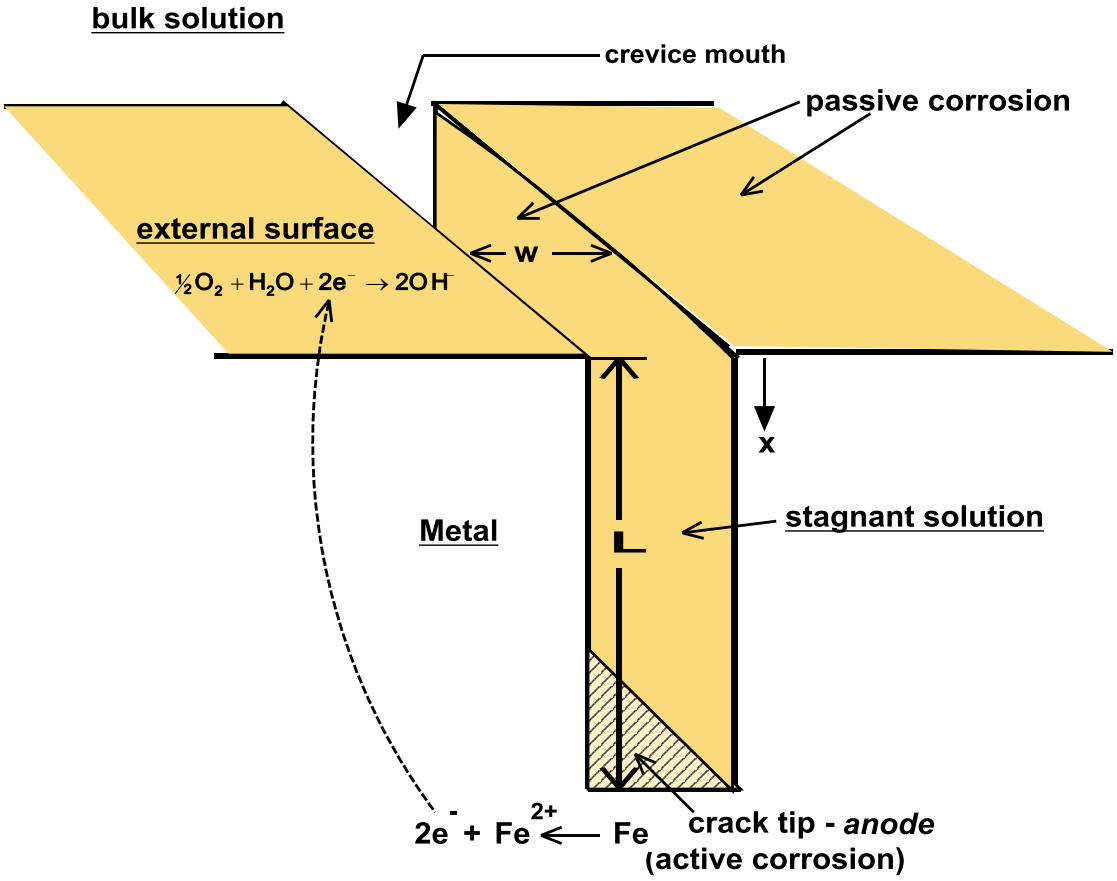


**Fig.14.24 Water-filled crevice in iron**

### 14.7.1 Mechanism

The sequence of steps that drives the corrosion processes inside a water-filled crevice include:

**1**. $O_2$ in the water in the crevice is depleted by reaction with the metal sides. The small width means that replenishment of $O_2$ requires molecular diffusion of this species from the crevice mouth through the stagnant water filling the length of the crevice, Diffusion is slow compared to the corrosion reactions occurring at the bottom.

**2.** The metal on the bottom of the crevice undergoes active corrosion:

$$Fe \rightarrow Fe^{2+} + 2e \tag{14.75}$$

The metal ion reacts with water, producing a variety of hydroxides. For the present analysis, only the production of solid iron oxide is considered:

$$Fe^{2+} + H_2O \rightarrow FeO + 2H^+ \tag{14.76}$$

The FeO is assumed to exist as a fine suspension of very small particles that does not impede diffusion of ionic species in the water in the crevice.

The net anodic (oxidation) process at the crevice bottom is the sum of the above two reactions:

$$Fe + H_2O \rightarrow FeO + 2H^+ + 2e \tag{14.77}$$

$H^+$ ions are produced by reaction(14.76) with consequent decrease in the pH of the solution at the base of the crevice. Because of the slow production rate of $OH^-$ on the external surface (Fig. 14.24), neutralization of $H^+$ is very inefficient.

**3**. The net result of metal dissolution in the crevice is generation of positive ions ($H^+$) at the crevice bottom. If the bulk solution contains a significant concentration of NaCl, for example, the $Cl^-$ concentration greatly exceeds that of $OH^-$ and is available to diffuse down the crevice to neutralize the excess positive charge of the $H^+$. This permits the corrosion reaction to continue. The walls of the crevice are assumed to be passivated and hence inert to the solution.

**4.** The electrons produced by reaction (14.75) at the crevice bottom are conducted through the metal to the surface contacted by the bulk water. Here $O_2$ is readily available, so the electrons produced at the crevice bottom are consumed by the $O_2$ cathodic half-cell reaction on the metal surface external to the crack (see Fig. 14.24).

The following analysis is based on the above mechanism, which is a simplified version of the model proposed by the Engelhardt et al (9) and Sharland (10).

### 14.7.2 Electrochemistry in the crevice

The important ionic pecies in the crevice solution are $H^+$, $Na^+$ and $Cl^-$ and $OH^-$. Dissolved $O_2$ is negligible for the reason given in No. 1 above. Likewise, $Fe^{2+}$ and ferrous hydroxides are not treated because once formed, they immediately react to precipitate FeO, as in Eq (14.76).

The aqueous analog of Eq (14.47) for the solution species are:

$$J_j = -D_j \frac{d[j]}{dx} - u_j[j]\frac{d\phi}{dx} \tag{14.78}$$

where j = $H^+$, $Na^+$, $Cl^-$. [j] is the molar concentration of species j. The diffusivity of component j in water is $D_j$ and $u_j$ is its mobility. $\phi$ is the electrode potential of the solution in the crevice at depth x. From Eq (14.47) the ionic mobility is:

$$u_j = \frac{z_j D_j}{R_g T / F} \tag{14.79}$$

where F is the Faraday constant (Sect. 2.10.1). The units of RT/F are Volts.

Inasmuch as steady-state is assumed for the solution in the crevice, the flux of $H^+$ at depth x is twice the negative of the rate of production of $Fe^{2+}$ by the corrosion reaction, (Eq (14.77)):

$$J_{H^+} = -2\frac{i_{Fe}}{z_{Fe}F'} \tag{14.80}$$

F' = 96,500 Coulombs/mole electrons. The minus sign accounts for the definition of positive $J_j$ in the downward direction while the corrosion reaction produces $H^+$ that moves upward. Because $H^+$ is only produced at the crack tip (and not along the crevice walls), $J_H$ is independent of x.

Because the fluxes of $Na^+$ and $Cl^-$ are everywhere zero,

$$J_{Na} = J_{Cl} = 0 \tag{14.81}$$

Combining Eqs (14.77) and (14.78) and expressing the fluxes by Eqs (14.80) and (14.81) yields:

$$D_H\left[\frac{d[H^+]}{dx} + \frac{1}{R_g T / F}[H^+]\frac{df}{dx}\right] = 2\frac{i_{Fe}}{z_{Fe}F'} \tag{14.82}$$

$$\frac{d[Cl^-]}{dx} + \frac{1}{R_g T / F}[Cl^-]\frac{df}{dx} = 0 \tag{14.83}$$

$$\frac{d[Na^+]}{dx} + \frac{1}{RT / F}[Na^+]\frac{d\phi}{dx} = 0 \tag{14.84}$$

$$\left[OH^-\right] = K_W / \left[H^+\right] \tag{14.85}$$

$\phi$ is the difference in solution potential between the crevice mouth and at depth x in the crevice. $K_W$ is the equilibrium constant for dissociation of $H_2O$.

The rate of reaction (14.75) at the crevice bottom (x = L) is given by the anodic Tafel relation, Eq (14.16):

$$\frac{i_{Fe}}{z_{Fe}F'} = \left(\frac{i_{oFe}}{z_{Fe}F'}\right)\exp\left(\frac{\alpha_{Fe}z_{Fe}}{RT/F}(\phi_M - \phi_L)\right) \qquad (14.86)$$

$i_{oFe}$ is the exchange current density for anodic half-cell reaction (14.75). $\phi_M$ is the known potential of the structural iron in which the crevice is located and $\phi_L$ is the electrode potential at the tip of the crevice (x= L) relative to that at the crevice mouth.

Finally, electrical neutrality requires:

$$\left[H^+\right] + \left[Na^+\right] = \left[OH^-\right] + \left[Cl^-\right] \qquad (14.87)$$

Equations (14.82)-(14.84) are rewritten as:

$$\frac{d\alpha}{d\eta} + \alpha\frac{d\Phi}{d\eta} = \frac{2\times10^3 i_{Fe}L}{z_{Fe}F'D_H[H^+]_0} \qquad (14.88)$$

The factor $10^3$ converts the units of concentration from moles/dm$^3$ (molarity) to moles/cm$^3$.

$$\frac{d\beta}{d\eta} - \beta\frac{d\Phi}{d\eta} = 0 \qquad (14.89)$$

$$\frac{d\chi}{d\eta} + \chi\frac{d\Phi}{d\eta} = 0 \qquad (14.90)$$

where:

$$\alpha = \frac{[H^+]}{[H^+]_0} \qquad \beta = \frac{[Cl^-]}{[NaCl]_0} \qquad \chi = \frac{[\mathrm{Na}^+]}{[NaCl]_0} \qquad (14.91)$$

$[H^+]_0$ is the hydrogen ion concentration in the neutral bulk coolant (and at the mouth of the crevice) and $[NaCl]_0$ is the concentration of sodium chloride impurity in the bulk coolant.

The dimensionless form of the voltage drop in the crevice is:

$$\Phi = \frac{\phi}{RT/F} \qquad (14.92)$$

and

$$\eta = x/L \qquad (14.93)$$

is the dimensionless distance from the crevice mouth.

The boundary conditions at the crevice mouth are:

$$\alpha = \beta = \chi = 1 \; at \; \eta = 0 \qquad (14.94)$$

The solution of Eqs (14.89) and (14.90) are:

$$\beta = e^{\Phi} \qquad \chi = e^{-\Phi} \qquad (14.95)$$

Next comes application of electrical neutrality (Eq (14.87)) [9]. Since Φ is positive, towards the tip of the crevice $[Cl^-] >> [Na^+]$ and the only ions at significant concentration are $H^+$ and $Cl^-$. Equation (14.87) reduces to:

$$\left[H^+\right] \approx \left[Cl^-\right] = \left[NaCl\right]_0 \times e^{\Phi} \tag{14.96}$$

or, with Eq (14.91) :

$$\alpha = \frac{[NaCl]_0}{[H^+]_0} e^{\Phi} \tag{14.97}$$

Substituting Eq (14.97) into Eq (14.88) gives:

$$e^{\Phi} \frac{d\Phi}{d\eta} = A \tag{14.98}$$

With the boundary condition $\Phi = 0$ at $\eta = 0$ the solution is:

$$\Phi = \ln\left(1 + A\eta\right) \tag{14.99}$$

Despite the electrical neutrality approximation in Eq (14.96), Eq (14.99) is correct at $\eta = 0$ and a good approximation as $\eta \rightarrow 1$ as long as A is large. The dimensionless constant A is:

$$A = \frac{10^3 L}{[NaCl]_0 D_H} \left( \frac{i_{Fe}}{z_{Fe} F'} \right) \tag{14.100}$$

Substituting Eq (14.86) into the above, along with $\Phi_L = \ln(1+A)$, yields:

$$A = \frac{10^3 L}{[NaCl]_0 D_H} \left( \frac{i_{oFe}}{z_{Fe} F'} \right) \frac{\exp(\alpha_{Fe} z_{Fe} \Phi_M)}{(1+A)^{\alpha_{Fe} z_{Fe}}} \tag{14.101}$$

The distribution of $H^+$ in the crevice is determined by the full electrical neutrality condition without the approximation in Eq (14.96). Assuming that the coolant is neutral water, Eq (14.88) becomes:

$$\frac{B}{\alpha} + e^{\Phi} = B\alpha + e^{-\Phi} \tag{14.102}$$

where:

$$B = \left[H^+\right]_0 / \left[NaCl\right]_0 \tag{14.103}$$

Equation (14.102) approaches the correct limit as $\eta = 0$ (where $\Phi = 0$ and $\alpha = 1$). As $\eta \rightarrow 1$, $\alpha$ and $\Phi$ become large, so that the first and the fourth terms become negligible and Eq (14.102) reduces to Eq (14.97).

The distributions in the crevice are determined as follows:

1. A is determined from Eq (14.101) for the system conditions and properties
2. The electrode potential $\Phi$ is determined as a function of location in the crevice from Eq (14.99).

3. The $Cl^-$ and $Na^+$ concentrations are computed from Eq (14.95)
4. The $H^+$ concentration ($\alpha$) is calculated as a function of $\eta$ from the solution of Eq (14.102):

$$\alpha = f(\Phi)\left[\sqrt{1+1/f^2(\Phi)}+1\right] \tag{14.104}$$

where

$$f(\Phi) = \frac{1}{2B}\left(e^{\Phi} - e^{-\Phi}\right) \tag{14.105}$$

At the crevice mouth, $\Phi \to 0$, $f(\Phi) \to 0$ so $\alpha \to 1$, in agreement with Eq (14.94).
At the crevice tip, $\Phi >> 1$, $f(\Phi) \to e^{\Phi}/2B >> 1$, so $\alpha \to 2f(\Phi) = e^{\Phi}/B$, which is Eq (14.96).

Example #8 Ion distributions in a crevice in iron at 25°C
Crevice depth L = 3 mm
Metal potential $\phi_M$ = - 0.2 V
$D_H = 1\times10^{-4}$ cm$^2$/s
Temperature T = 25°C
Neutral bulk water $[H]_0 = 10^{-7}$ M
Salt concentration $[NaCl]_0 = 10^{-4}$ M
exchange-current density $i_{oFe} = 10^7$ A/cm$^2$
anodic symmetry factor $\alpha_{Fe} = 0.5$
valence $z_{Fe} = 2$

From Eq (14.92), the dimensionless electrode potential of the iron structure in which the crevice is located is:

$$\Phi_M = \frac{\phi_M}{RT/F} = \frac{-0.2}{8.314\times300/96.5\times10^3} = -\frac{0.2}{0.026} = -7.7$$

The parameter A is determined by Eq (14.101):

$$A(1+A) = \frac{10^3\times0.3}{10^{-4}\times10^{-4}}\left(\frac{10^7}{2\times96{,}500}\right)\exp(-7.7) = 6\times10^8$$

which yields:

$$A \cong \sqrt{6\times10^8} = 2\times10^4$$

Equation (14.99) becomes:

$$\Phi = \ln(1+2\times10^4\,\eta)$$

Converting to the dimensional potential by Eq (14.92), the distribution of $\phi$ is plotted in Fig. 14.25.

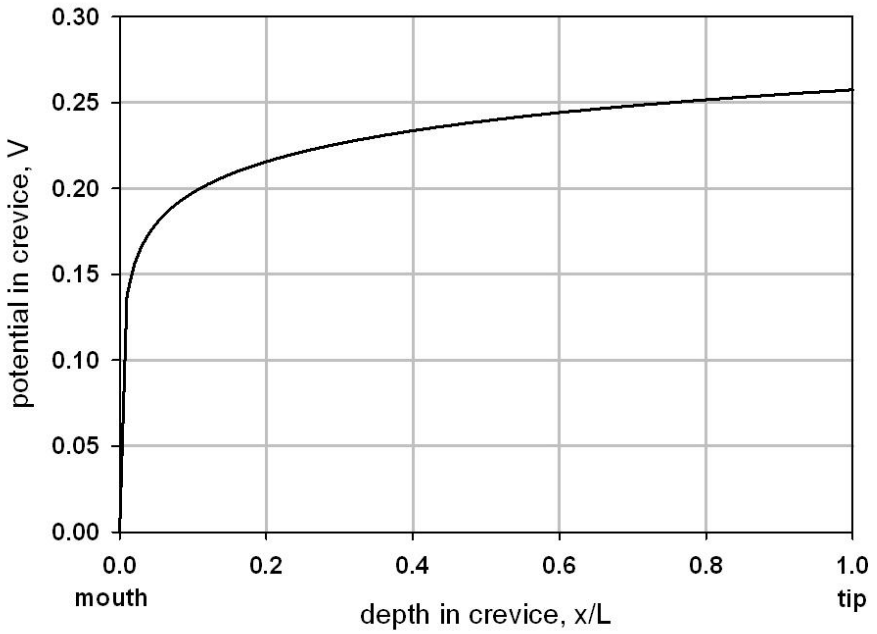


**Fig. 14.25 Electrode potential in crevice solution (relative to value at the mouth)**

The concentrations of the four ionic species in Eq (14.88)-(14.90)are determined next. $[Cl^-]$ and $[Na^+]$ follow from Eq (14.95) and the last two of Eqs (14.91):

$$\beta = e^{\Phi} = 1 + 2\times10^4\eta \sim 2\times10^4\eta; \quad [Cl^-] = 10^{-4}\beta = 2\eta;$$

$$\chi = e^{-\Phi} = \frac{1}{1+2\times10^4\eta} \cong \frac{1}{2\times10^4\eta}; \quad [Na^+] = 10^{-4}\chi = \frac{5\times10^{-9}}{\eta}$$

$\alpha$ is obtained from Eqs (14.104) and (14.105) and from Eq (14.103), $B = 10^{-7}/10^{-4} = 10^{-3}$. Equation (14.105) becomes: $f(\Phi) = 500(e^{\Phi} - e^{-\Phi})$. Except for $\eta$ very close to zero, where $\Phi \to 0$, $f(\Phi) \sim 500e^{\Phi} = 500(1 + 2\times10^4\,\eta) \sim 10^7\eta$. With $f(\Phi) >> 0$, Eq (14.104) reduces to $\alpha = 2f(\Phi) = 2\times10^7\eta$. Converting this result to concentration units (molarity) by the first of Eqs (14.91)

$$[H^+] = 2\eta$$

$[OH^-]$ follows from Eq (14.85).

The concentration profiles are shown in Fig. 14.26. The approximation of Eq (14.96) applies for $\eta > 0.01$. At $\eta = 0$, $[Cl^-] = [Na^+] = 10^{-4}$ M and $[H^+] = [OH^-] = 10^{-7}$ M.

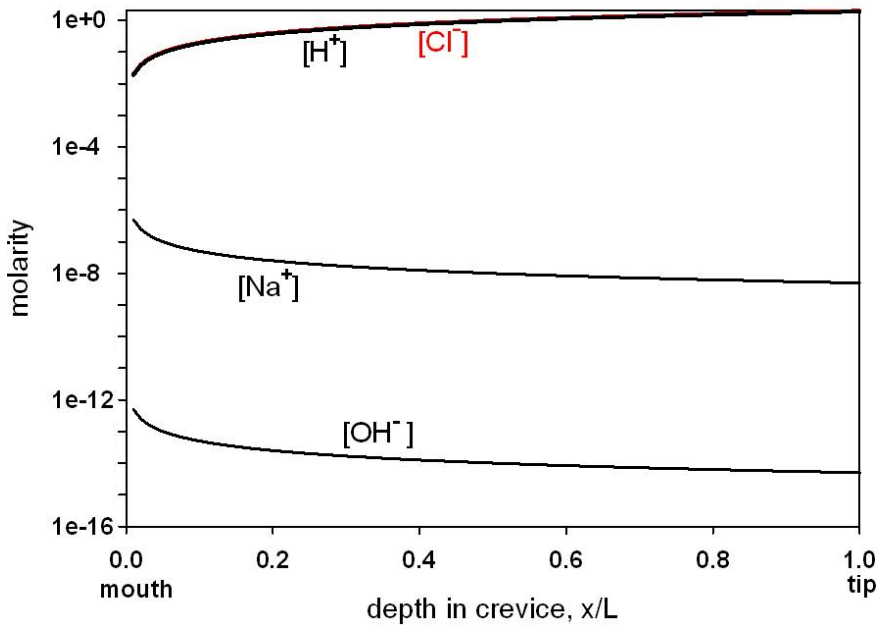


**Fig. 14.26 Concentration profiles of ions in crevice for $\eta > 0.01$**

### 14.7.3 Computational results

Figures 14.27 and 14.28 result from a more complete analysis of the chemistry of the crevice [10]. The calculations underlying the curves include active corrosion along crevice walls, which was neglected in the simple model presented in the previous section. Also, two iron ions, $Fe^{2+}$ and $FeOH^{+}$ are included among the ionic products of corrosion of the metal. In the previous section, these ions were assumed to react rapidly with water to produce the solid oxide (reactions (14.75) and (14.76) )) .

The electrode potentials are similar in shape to that in Fig. 14.25 (the directions of the abscissas are reversed); rapid changes near the mouth decreasing greatly on approaching the tip. The increase in electrode potential in the crevice and the low pH leads to active corrosion (see Fig. 14.1).

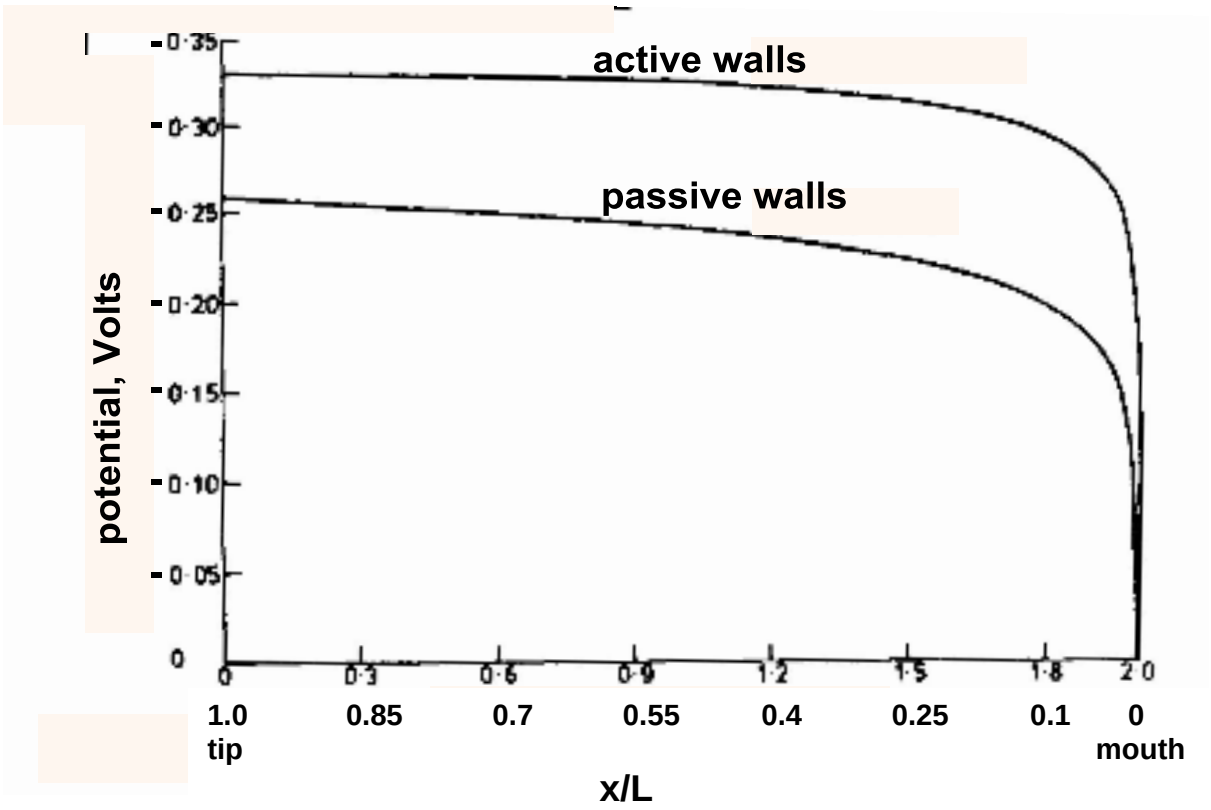


**Fig. 14.27 Potential profiles in a 2-mm-long crevice with the following conditions: $\phi_o$ = 0 V; $[NaCl]_o$ = 0.02 M; pH = 7. From Ref. 10**

The important features of the curves in Fig. 14.28 are:
(a) sharp changes occur within 5% of the crevice mouth; by x/L ~ 0.1 the curves become essentially flat, indicating only minor concentration changes.
(b) The pH is ~ 4.5 over most of the length of the crevice, falling to the bulk water pH = 7 only very near the crevice mouth. Due to neglect of the iron ions in Fig. 14.26, the solution in the crevice of approaches pH = 0 at the tip. The consequence of the simultaneous decreases in pH and increases in electrode potential from the crevice mouth to the tip can be seen on the Pourbaix diagram (Fig. 14.1). The thermodynamically-stable chemistry changes from an oxide to $Fe^{2+}$, which promotes active corrosion.
(c) The combination of the concentrations of $Fe^{2+}$ and $Fe(OH)^{+}$ along the crevice causes a high $Cl^{-}$ concentration (~ 0.5 M) to provide solution neutrality.
(d) $Na^{+}$ has been pushed out of the crevice.

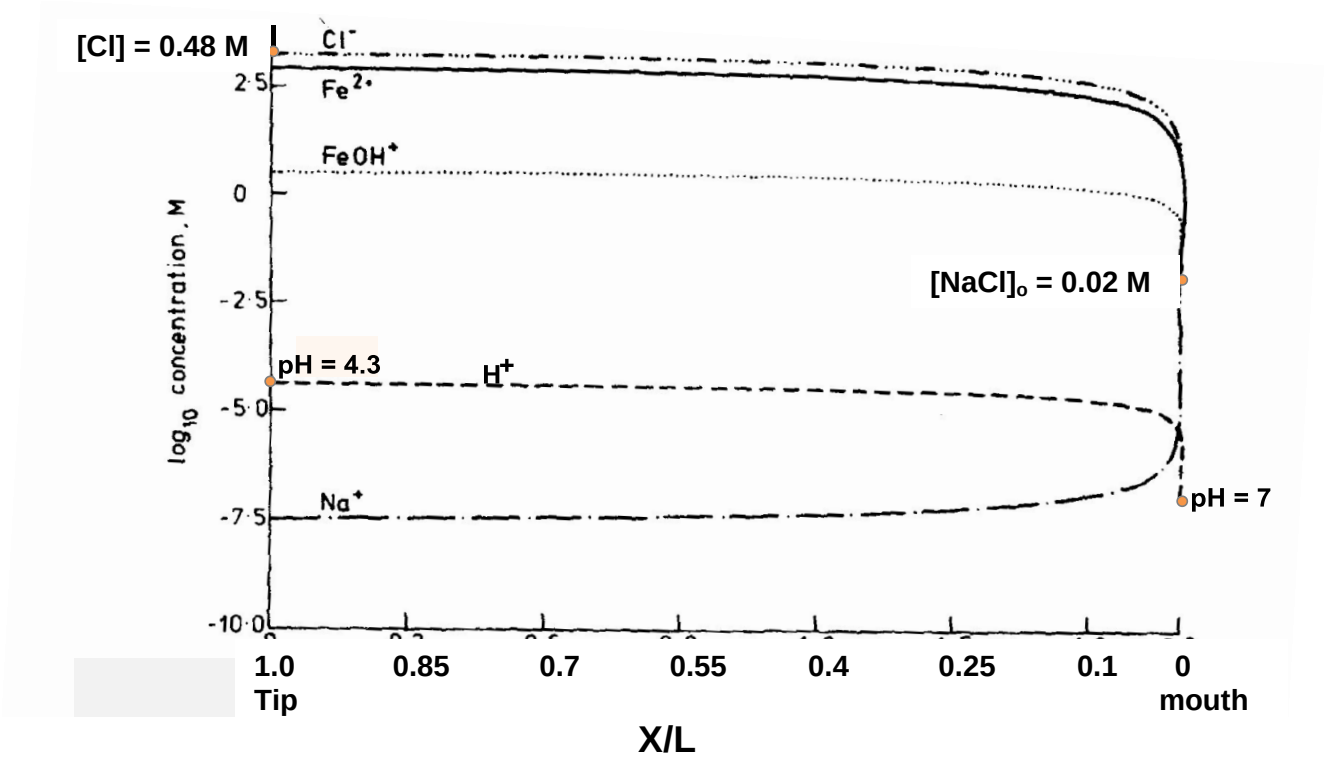


**Fig. 14.28 Concentration profiles in a 2-mm-long crevice. Active corrosion on walls After Ref. 10**

### 14.7.4 Improvements of the model

i) cathodic half-cell reactions (e.g., $H^+ + e^- \rightarrow \frac{1}{2} H_2$) along the crevice walls

ii) aggressive anions other than $Cl^-$ in the bulk water (e.g., $SO_4^{2-}$);

iii) restricted diffusion of ions in the water in the crevice by precipitation of oxide (e.g. by reaction (14.76)) - the solubilities in water of ionic species of iron, nickel and chromium are very low;

iv) concentration and electric potential gradients in the bulk water, as in Ref. 9.

vii) trapezoidal rather than the rectangular crevice shape shown in Fig. 14.24. This modification is necessary when the method is applied to a crack in the metal rather to a crevice formed by a gap between two metal pieces **[11].**

viii) transient crevice corrosion (i.e., growth of a crack)

ix) Inclusion of solubility limits of all metal ions in solution in the crevice water [**12]**

## References


1. J. Newman, *"Electrochemical Systems"*, pp. 12 - 21, Chaps. 3, 8, 11 and 16, Prentice-Hall Inc. (1973) and later editions.

2. P. Marcus, Ed, *Corrosion Mechanisms in Theory & Practice*", 2nd Ed, Chaps. 1, 6, 8, 11, m 12, Marcel Dekker (2002)

3. J. Scully, "*The Fundamentals of Corrosion"*, 2nd Ed. , Chap. 2, Pergamon Press (1981)

4. P. Atkins, *"Physical Chemistry"*, pp. 326 - 331, Chap. 29, W. H. Freeman (1978)

5. S. Ziemniak et al , Corr. Sci. **44** (2002) 2209; **45** (2003) 1595; **48** (2006) 2525; **48** (2006) 3330

6. G. Bohnsark, *"The solubility of Magnetite in Water and in Aqueous Solutions of Acid and Alkali"*, Hemisphere Publishing Corp. (1988)

7. F. Sweeton & C. Baes, Jr, *"The solubility of magnetite and hydrolysis of ferrous ions in aqueous solutions at elevated temperatures"*, J. Chem. Thermodynamics **2** (1970) 479

8. A. T. Fromhold, *Solid-State Ionics*, **75** (1995) 229

9. G. Engelhardt et al, *"Fast algorithms for estimating stress-corrosion crack- growth rate"* Corr. Sci. **41** (1999) 2267

10. S. Sharland, "*A mathematical model of crevice and pitting corrosion II"* Corrosion Sci. **28** (1989) 621

11. S. Sharland,, *"A review of theoretical modeling of crevice and pitting corrosion"* Corrosion Sci. **27** (1987) 289

12. A.Tucker & J. Thomas, *"A model of crack electrochemistry for steels in the active state based on mass transport by diffusion and ion migration"* J. Electrochem. Soc. **129** (1982) 1412

13. A. Couet, A.T. Motta, A. Ambard, "*The Coupled Current Charge Compensation Model for Zirconium Alloy Fuel Cladding Oxidation: I.Parabolic Oxidation of Zirconium Alloys"*, Corrosion Science (in press), (2015).

14. J. Bischoff and A. T. Motta, *"Oxidation behavior of ferritic-martensitic and ODS steels in supercritical water,"* Journal of Nuclear Materials, **424**, (2012) 261-276.

# Problems Chap. 14

**14.1**

Look up the Gibbs energy of formation of $H_2O$(liq) from the web site of the National Institute of Standards (kinetics.nist.gov/janaf/). At 25°C, show that this value is consistent with the standard electrode potential No. 1 in Table 2.2.

**14.2**

Water at pH 7 fills a glass container.

The pertinent half-cell reactions and their standard electrode potentials and exchange current densities are:

| j | Half-cell Reaction | $\phi^o$, V | $i_o$, A/cm$^2$ |
|---|---|---|---|
| 1. | $½O_2 + 2H^+ + 2e = H_2O$ | 1.23 | 2e-6 |
| 2. | $H_2O_2 + 2H^+ + 2e = 2H_2O$ | 1.77 | 4e-8 |
| 3. | $2H^+ + 2e = H_2$ | 0 | 4e-8 |

Water is saturated with $O_2$ at 0.5 atm and $H_2$ at 0.1 atm and has an $H_2O_2$ concentration of $10^{-3}$ M. The symmetry parameters (Sect. 14.4.4) are 0.5 for all half-cell reactions. What is the electrochemical potential (ECP) of the water? There are no reactions with the container surface.

**14.3**

A piece of iron is immersed in water containing:

$[Fe^{2+}] = 0.1$ M

$[H_2] = 10$ ppm (wt)

pH = 2

The Tafel lines are:

$i_{oH} = 10^{-6}$ A/cm$^{2;}$ ; $i_{oFe} = 10^{-7}$ A/cm$^2$

$\beta_H = \beta_{\Phi\varepsilon} = 0.5$ (see Eqs (14.16) nd (14.17))

(a) What is the electrochemical potential of the system?
(b) According to the Pourbaix diagram (Fig. 14.1), should iron corrode?
(c) What is the corrosion rate in mm/yr?

**14.4**

$O_2$ dissolves in water according to Henry's law: $K_{Hen} = 0.03$ (25°C);

$$K_{Hen} = p/[i]$$

p is the pressure of the gaseous species in atm. [i] is the concentration in water in ppm by weight.

(a) What is the electrochemical potential of neutral water containing 5 ppm by weight of $O_2$?
(b) According to Fig. 14.1, what is the stable phase of iron in neutral water at 25°C?

**14.5**

$$2/3Fe_3O_4 + 4H^+ + 2/3H_2 = 2Fe^{2+} + 8/3H_2O$$

(a) What is the half-cell reaction corresponding to the $Fe_2O_3$/ $Fe_3O_4$ \line on the Pourbaix diagram of Fig. 14.1?
(b) What is the standard electrode potential of the half-cell reaction of (a)?
(c) What is the value of the equilibrium constant for the above reaction (K)?

**14.6**

Construct the Pourbaix diagram for the cadmium-water system based on the following:

1. $Cd = Cd^{2+} + 2e$ $\quad \phi_1^o = -.403$

2. $Cd + 2H_2O = HCdO_2^- + 3H^+ + 2e$ $\quad \phi_2^o = .583$

3. $Cd + H_2O = CdO + 2H^+ + 2e$ $\quad \phi_3^o = .005$

4. $Cd^{2+} + H_2O = CdO + 2H^+$ $\quad K_4 = 10^{-13.8}$

5. $CdO + H_2O = HCdO_2^- + H^+ + 2e$ $\quad K_5 = 10^{-19.5}$

Include the water decomposition lines (a) and (b) in Fig. 14.1.
Indicate regions of corrosion, immunity and passivity.

**14.7**

The corrosion situation described in Prob. 14.3 takes place in a liquid volume V and an iron specimen of surface area A. The $Fe^{2+}$ and $H^+$ concentrations are initial values. As corrosion proceeds, the former increases and the latter decreases,, so $i_{corr}$ decreases with time.
What are the equations from which $[Fe^{2+}]$, $[H^+]$ and $i_{corr}$ can be calculated? Do not attempt to solve.

**14.8**

Cathodic reduction of $O_2$ dissolved in water is limited by concentration polarization. Calculate the mass-transfer limited corrosion rate (mm/yr) of iron in an aqueous solution containing 40 ppm (by wt) dissolved oxygen. The diffusion coefficient of $O_2$ in water is $10^{-8}$ $cm^2/s$ and the stagnant film in the specimen is 100 μm thick.

**14.9**

The pH of the coolant water in a PWR affects corrosion of zirconium based cladding in part by controlling the aqueous concentration of zirconium ions according to the reaction:

$$ZrO_2(s) + 4\,H^+ = Zr^{4+} + 2H_2O$$

(a) What is the equilibrium constant for this reaction at 400 C obtained from the following information:

$$Zr = Zr^{4+} + 4e \qquad \varepsilon^o = -1.53eV$$
$$Zr(s) + O_2 = ZrO_2(s) \quad \Delta\mu^o = -227kcal/mole$$
$$2\,H_2(g) + O_2(g) = 2H_2O \quad \Delta\mu^o = -93kcal/mole$$

(b) If the coolant is made basic by addition of 10-4 mole/l of LiOH what is the equilibrium concentration of zirconium ions in the coolant? The dissociation of water at 400 C is 10-11.

(c) at what pH would “significant corrosion” (in the sense used in the Pourbaix diagrams) of oxide covered Zircaloy occur?